TECHNISCHE UNIVERSITÄT WIEN

NUCLEAR ENGINEERING SEIBERSDORF

Investigations of a Waste Simulate Contaminated with Cs-137 in the Context of Real Radioactive Waste

DIPLOMARBEIT

zur Erlangung des akademischen Grades

Diplom-Ingenieurin

eingereicht von

Petra Holzer, B.Sc.
Matrikelnummer 11808367

an der Fakultät für Physik

der Technischen Universität Wien

Betreuung: DI Dr. Dirk Vulpius
Privatdoz. DI Dr.techn. Johannes H. Sterba

Johannes H. Sterba

Dirk Vulpius

Wien, 6. August 2025

Petra Holzer

TECHNISCHE UNIVERSITÄT WIEN

NUCLEAR ENGINEERING SEIBERSDORF

Investigations of a Waste Simulate Contaminated with Cs-137 in the Context of Real Radioactive Waste

DIPLOMA THESIS

submitted in partial fulfillment of the requirements for the degree of

Diplom-Ingenieurin

by

Petra Holzer, B.Sc.
Registration Number 11808367

to the Faculty of Physics

at the TU Wien

Advisors: DI Dr. Dirk Vulpius
Privatdoz. DI Dr.techn. Johannes H. Sterba

Johannes H. Sterba

Dirk Vulpius

Vienna, August 6, 2025

Petra Holzer

Erklärung zur Verfassung der Arbeit

Petra Holzer, B.Sc.

Hiermit erkläre ich, dass ich diese Arbeit selbständig verfasst habe, dass ich die verwendeten Quellen und Hilfsmittel vollständig angegeben habe und dass ich die Stellen der Arbeit – einschließlich Tabellen, Karten und Abbildungen –, die anderen Werken oder dem Internet im Wortlaut oder dem Sinn nach entnommen sind, auf jeden Fall unter Angabe der Quelle als Entlehnung kenntlich gemacht habe.
Ich erkläre weiters, dass ich mich generativer KI-Tools lediglich als Hilfsmittel bedient habe und in der vorliegenden Arbeit mein gestalterischer Einfluss überwiegt. Im Anhang „Übersicht verwendeter Hilfsmittel“ habe ich alle generativen KI-Tools gelistet, die verwendet wurden, und angegeben, wo und wie sie verwendet wurden. Für Textpassagen, die ohne substantielle Änderungen übernommen wurden, habe ich jeweils die von mir formulierten Eingaben (Prompts) und die verwendete IT- Anwendung mit ihrem Produktnamen und Versionsnummer/Datum angegeben.

Wien, 6. August 2025

Petra Holzer

Danksagung

Ich bin äußerst dankbar für alle Leute, die nur das Beste für mich wollten und mich während der letzten Schritte in meinem Studium so sehr unterstützt haben.

Mein größter Dank gilt bestimmt Dirk, der unheimlich viel Zeit mit mir verbracht hat, um mich zu unterstützen. Danke dafür, dass ich so viel von dir lernen durfte und du so viel Geduld mit mir hattest. Weiters möchte Andreas Vesely danken, der uns selbst dann weiterhelfen konnte, wenn wir mit unserem Latein am Ende waren. Besonders dankbar bin ich für das Umfeld, das ich bei NES erleben durfte. So viele Leute haben mir während meines Jahres bei ihnen auf unterschiedlichste Art und Weise geholfen. Überhaupt bin ich dankbar für diese Chance meiner Abschlussarbeit bei NES.

Danke Johannes für deine angenehme Betreuung und dein wertvolles Feedback. Danke, dass du immer problemlos für mich da warst und unkompliziert Hilfe anbieten konntest. Deine Meinungen und Empfehlungen haben mir viel bedeutet.

Die lieben Menschen, die ich während meiner Zeit an der Uni kennenlernen durfte, haben diese Jahre zu etwas ganz Besonderem gemacht. Ich bin stolz darauf, dass ich mich in diesem Umfeld entfalten konnte.

Last but never least, meine Familie, der ich sowieso alles zu verdanken habe.

Abstract

A key challenge in the treatment of radioactive waste is the representative analysis of inhomogeneous materials. Specifically, sampling as well as inhomogeneity have a high impact on results, making it difficult to characterize large material flows correctly in terms of their chemical and physical properties.

Gamma spectroscopy of gravel artificially contaminated with ^{137}Cs has shown unexpected deviating activity concentrations. Investigations into material properties, such as particle size, mineral composition or differences resulting from the contamination method, provide insights into the activity distribution within the material. Grinding proves to be the most reliable method for homogenizing samples when working with small amounts.

Further analysis of real radioactive waste support the insights gained from the waste simulate. Furthermore, with regards to the diverse radionuclide inventory of real waste, the quantification of β-emitters was substantially improved. Chemical separation of radioisotopes is being investigated, however adapted spectrum analysis can partially achieve similarly accurate results.

Kurzfassung

Bei der Behandlung von radioaktiven Abfällen stellt die repräsentative Analyse von inhomogenen Stoffen eine große Herausforderung dar. Besonders die Probennahme sowie Inhomogenitäten in der Probe beeinflussen die Ergebnisse aus der Analyse und erschweren es, große Materialströme bezogen auf ihre chemischen und physikalischen Eigenschaften korrekt zu charakterisieren.

Gammaspektroskopie von absichtlich mit ^{137}Cs kontaminiertem Schotter hat unerwartet siginifikante Abweichungen in der Aktivitätskonzentration ergeben. Untersuchungen der Materialeigenschaften, wie Partikelgröße, mineralogische Zusammensetzung oder durch die Kontaminationsmethode verursachte Unterschiede, geben Aufschluss über die Aktivitätsverteilung im Material. Mahlen erweist sich als die zuverlässigste Methode zur Homogenisierung von groben Proben, wenn mit kleinen Probenmengen gearbeitet wird.

Weitere Analysen eines realen radioaktiven Abfalls stützen die Erkenntnisse, die aus dem Schottersimulat gewonnen wurden. Darüber hinaus wurde im Hinblick auf das vielfältige Radionuklidinventar des realen Abfalls die Quantifizierung der β-Strahler verbessert. Die chemische Trennung von Radioisotopen wird derzeit untersucht, jedoch kann ein angepasstes Auswerteverfahren teilweise ähnlich genaue Ergebnisse erzielen.

Contents

Chapter 1

Introduction

This study is focused on the question of sufficient homogeneity in samples and the investigation of certain measurement methods currently applied at Nuclear Engineering Seibersdorf (NES) laboratories, which are linked and compared to each other. Therefore, inhomogeneities in the ^{137}Cs activity concentration in contaminated gravel are investigated thoroughly and compared to real radioactive waste of the recondition program. An overview of the most influential properties is provided. The impact of treatments to achieve greater homogeneity, such as grinding, is also examined.

Additionally, measurement methods like gamma spectroscopy and X-ray fluorescence spectroscopy (XRF) are compared and linked. Extended radiometric analysis is carried out by using liquid scintillation counting (LSC) to investigate β-emitters in radioactive waste. Current LSC methods are reviewed and improvements are investigated.

As sampling determines the outcome of analysis directly, the influence of inhomogeneities needs to be investigated more intensively. Accurate material characterization in radioactive waste management is essential due to the demand of proper documentation and appropriate further treatment. For NES, reliable characterisation of samples, especially those from the reconditioning process, is important for both daily operations and future requirements. Drums are currently filled and conditioned with the expectation that they meet the acceptance criteria for future disposal.

Chapter 2

Theory

2.1 Radioactive Waste Management in Austria

In Austria, Nuclear Engineering Seibersdorf GmbH (NES) conducts the whole management and storage of radioactive waste. Austria signed the joint convention on the safety of spent fuel management and on the safety of radioactive waste management, which established safety regulations and a peer review system [1]. NES is responsible for the conditioning and interim storage of low and intermediate level radioactive waste. High level waste does not arise and therefore does not have to be treated in Austria and will not be of concern in regarding a future disposal facility. A disposal facility for radioactive waste does not exist and is not under construction. There are several facilities and instruments at NES, which serve the purpose of receipt, conditioning and a safe and secure storage of radioactive waste. Conditioning must fulfill the tasks to bring waste into a stable form and reduce volume. The most important facilities are the waste water treatment facility, an incinerator and the new handling centre with a drum drying system, a supercompactor and other equipment for an ideal material flow [1].

In order to minimize waste and make the analysis of huge amounts of soil, gravel and concrete possible, a soil sorting facility was installed. Material similar to the gravel analyzed in this study is examined there. Fine or course grained material can be evaluated and sorted into not or barely contaminated and more contaminated waste. For this purpose, the material is placed on a belt and analyzed for β- and γ-emitters and is then directly sorted. The goal is to separate material with activities under the restricted clearance threshold and to take it out of the radioactive waste inventory, which reduces volume dramatically.

As mentioned, the current storage for radioactive waste is located on the site. After conditioning, all radioactive waste is stored in the so-called interim storage until an Austrian disposal is built and put into operation. The waste is deposited in drums in an air-conditioned environment. Depending on the dose rate, the weight or other radiological and chemical hazards, drums are stored in different positions of the racks to optimize safety.

2.1.1 Reconditioning

In addition to the processing of routine waste, waste drums from the past are reopened, characterized and reconditioned. Many of these drums date back to the 1970s and 1980s, when collection and storage of radioactive waste started at the facility in Seibersdorf. Nowadays they can be analyzed with today's state of technology. As a result, great

amounts of the content are cleared and can be pulled out of the radioactive waste inventory, which minimizes waste volume. The material, which is reconditioned, is stored in drums according to current standards.

The reconditioning of historic drums is part of the agreement [2] with the Republic of Austria to ensure the safe treatment and interim storage of all Austrian radioactive waste. One of the most important advances in the storage system, compared to the historic ones, is that all drums lay horizontally in racks and that each can be inspected at any time.

Ongoing projects are the repackaging of homogeneously and inhomogeneously cemented drums. The first one mostly consists of cemented ashes and sludges and the second describes 100-Liter drums with raw waste, which were cemented in 200-Liter drums. The inhomogeneously cemented drums date back to a time where possibilities for waste treatment were less efficient, i.e., no adequate high pressure press and no incinerator facility for volume reduction were available. Through this project approximately 60% of the volume could be reduced. When needed, samples are taken of these historic drums during repackaging and analysed in the on-site laboratories for their chemical and radiological properties. Since documentation is not always existing to a sufficient extend for drums conditioned decades ago, characterization and gaining new knowledge about the material is crucial for further handling.[2]

2.1.2 Example Origin of Radioactive Waste from the Site

A non-negligible part of radioactive waste at NES origins from the site itself, specifically from the past and previous works. One of the now decommissioned buildings on the site was the so-called Schlammbeethalle [3], Figure 2.1, a shack where sludge from the decontamination of active liquids was dried up. Already before 1990 the shack was taken out of service, in 2002 decommissioning was started and the site was completely restored to a field in 2006. Therefore, a huge amount of several components of the building had to be analyzed and conditioned. Most of the concrete was cleared and was stored in a conventional disposal site, since the contamination was mainly linked to the surface and was removed. Only in some cases a higher activity was found beneath different concrete layers, which suggests that previous contamination was covered up by new material [3].

The floor consisted mainly of the already mentioned concrete layer and bricks on top. Underneath one could find a gravel bed which showed at least partial contamination and was therefore handled and stored as radioactive waste above the clearance limit. The gravel waste which is analyzed during this study was taken from this Schlammbeethalle and likely originates from the region underneath the concrete and brick layers.

Figure 2.1: Schlammbeethalle before dismantling [3].

2.2 Properties of Cesium-137

Cesium belongs to the alkali metal group, is extremely reactive and is therefore mostly found in chemical bindings. It is analogous in its chemical behavior to potassium, which plays a role in the cesium uptake in plants and human muscle tissue [4]. Through the intake of cesium into the body, Cs^+ ions might even replace K^+ ions in certain constructs and block potassium channels [5]. Furthermore, cesium shows a volatile behavior when exposed to high temperatures [6, 7].

Only one stable isotope of cesium, ^{133}Cs exists in nature, all other are of anthropogenic origin. One of these is ^{137}Cs, one of the most common fission products of ^{235}U, which is of great interest in radioactive waste treatment and environmental pollution due to its long half-life of 30.02 years [8]. After a β^- decay to ^{137m}Ba, a γ ray with 661.665 keV is emitted and the nuclide relaxes to the stable ^{137}Ba [8].

2.2.1 Cesium Dynamics in the Environment

Cesium's high solubility causes potential environmental hazards because it offers possibilities to migrate into ground water and plants [9]. Especially in examinations for a suitable future disposal location, minerals acting as cesium adsorber are of great interest.

Due to nuclear accidents, huge amounts of radiocesium were released into the environment, which led to great interest in cesium dynamics and accumulation in soil, air and vegetation [10]. The hazard of ^{137}Cs release into the environment serves as motivation for investigations on its optimal removal [11].

Through the fact that ^{137}Cs is one of the major fission products of uranium, its adsorption on soil gets a lot of attention. Its radiological hazard and its half life lead to an extensive interest in cesium removal technologies and publications related to these methods have increased after Fukushima accident in 2011 [12]. Uptake models of Cs^+ in context of potassium ions in soil are investigated and because of its chemical similarity, cesium uptake into plants plays a role [13]. In soil itself, specially clay minerals and micas are assumed to contribute to cesium adsorbtion [14].

2.2.2 Adsorption Capacities of Certain Minerals

Cesium adsorption onto minerals, which happens via ion exchange, was investigated intensively for example with rocks, soil, pure or synthetic minerals [9]. There are studies on the adsorbtion of cesium onto common minerals found in soil, i.e., onto the surface of quartz [15, 16].

The capability of zeolites and their specific configurations to work as ion-exchangers is well known [17] and established in industrial applications like agriculture, radioactive waste treatment and disposal processes [18]. Investigations of natural and synthetic zeolites regarding their efficiency and improvements in use are the object of current research, especially for the adsorption of Cs^+ and Sr^{2+} because of their relevance in radioactive waste treatment [19, 20]. Since the removal of ^{137}Cs from radioactive waste is of great interest, zeolites [21, 22] and other adsorbing minerals [23] are investigated.

Despite ion exchangers like zeolite, micas like biotite and muscovite are associated with high selectivity for cesium and strontium as well [24]. K-depleted muscovite can exchange Cs^+ into the interlayers of the mineral structure and was observed to show high selectivity for Cs^+ [24]. Due to weathering processes Cs^+ can sorb to frayed edges and even diffuse into the crystal along cracks and defects, which might happen with muscovite in soil [25].

2.3 Measurement Methods

Several measurement methods are of great importance for this study and important aspects and theoretical concepts of the used methods will be discussed in the following.

2.3.1 Gamma Spectroscopy

Semiconductor detectors are widespread detector systems and often used to measure gamma radiation with high energy resolution. Germanium is an element with semiconductor properties which means that its valence electrons are bound to the atom with a certain energy. This certain amount of energy can release the valence electron and bring it to the conduction band. In the conduction band the electrons are not part of a

specific atom but rather a region with overlapping energy levels. This can happen through ionizing radiation by nuclear reactions and leaves a so called electron hole pair. The holes in this system mean the lack of electrons and they drift towards the cathode like the electrons move towards the anode. Germanium detectors must be cooled in order to avoid valence electrons moving to the conduction band by thermal motion, to improve energy resolution and minimize electrical noise. The threshold for germanium at $80\,K$ is $0.75\,eV$ but in reality it is $2.95\,eV$ due to energy loss as crystal excitation [26]. High Purity Germanium detectors (HPGe) are commonly used. Germanium has properties like a high atomic number thus it is denser and takes up ionizing radiation more easily than silicon [26].

A typical ^{137}Cs spectrum visualized by the software Genie2000 is depicted in Figure 2.2. Characteristic phenomena of a gamma spectrum are visible. The highest peak at $661.7\,keV$ is produced by photoelectric absorption of an incoming gamma-ray in the absorber material. A photoelectron is emitted and resulting vacancies in the electron shell are filled by stronger bound electrons. Compton scattering occurs when a photon is not absorbed completely but scattered at the electron shell. There exist two extreme cases, the first occurs when the gamma-ray is only scattered in a negligible angle and maintains almost all energy. In the second case, the gamma-ray is scattered back in its original direction and the maximum energy is transferred to an electron. These electrons are observed in the spectrum as Compton background. Furthermore, gamma-rays, which are scattered in the shield, can be scattered back to the detector resulting in the backscatter peak. [27]

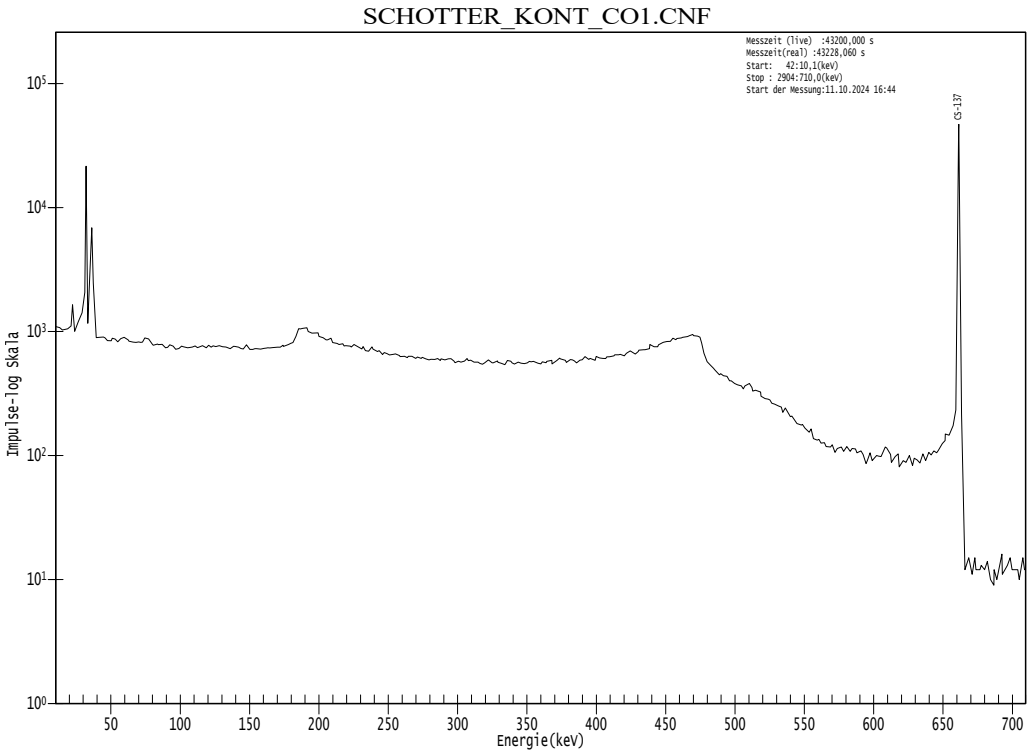

Figure 2.2: Spectrum recorded of the 661.7 *keV* photo peak of gravel containing ^{137}Cs. Counts are in log scale for better visibility of the structures in the spectrum. Lowest peaks are generated due to X-ray emissions. Backscatter peak close to 200 *keV*, the Compton edge around 460 *keV* and the whole Compton continuum, introduced by compton effects in the detector, are visible. The characteristic full energy photo peak of ^{137}Cs is visible in the high energy edge of the spectrum. Measuring time was too short to detect photo peaks of other nuclides of natural origin, as seen in Figure 3.5.

2.3.2 Liquid Scintillation Counting (LSC)

Other than the semiconductor method used before, LSC is based on a scintillation detector and works with the luminescence of molecules. The analyte, i.e. the radionuclides in the gravel, needs to be brought into solution. A scintillator, which is usually found as a liquid cocktail adapted for LSC purposes, contains certain molecules, which, when excited by electrons of β decay, emit photons in the visible or ultraviolet spectrum when de-exciting to lower energy levels or the ground state. These photons can mostly pass the cocktail molecules without absorption because their excitation energy is much higher, which is crucial to reach the photomultiplier tube (PMT). It goes without saying that the sample chamber including the scintillator and the PMT must be shielded from light [26].

The scintillator itself has to fulfill certain properties in order to lead to measurement results. Since a broad spectrum of analytes is analysed with LSC, cocktails are adapted for different demands and are used depending on the analyte and measuring goals. The most important property is, that the scintillator has to be transparent to its own emitted photons but must absorb the emitted particles of the analyte quite well. Furthermore the emitted photons should occur with a high efficiency and be detectable for the photomultiplier, which only happens in a specific wavelength range, i.e. the region where the PMT is sensitive. To achieve the latter, wave-length shifters might be added to the cocktail [26]. Aromatic organic molecules work well and are often used as LSC solvents [28].

Quenching

Molecules other than the scintillator interact with photons and prevent them from reaching the PMT. A reduction of efficiency can occur. This effect, mainly caused by chemical reactions or changes in optical properties, is called quenching. Chemical quenching hinders the production of a light signal for the PMT when heat is produced instead of photons. Color quenching happens when photons from the scintillator are mitigated by colored contents [26]. In figure 2.3 samples prepared with different components and nitric acid ratios are shown. Directly after preparation no distinction between the four vials containing 15 ml of cocktail was possible but three months later an intense yellowish darkening has developed. Although no optical difference was visible, LSC spectra obtained by measurements right after preparation did already show quenching effects.

Figure 2.3: From left to right: Pure digestion solution for Cerenkov counting, blank sample, 1 ml, 2 ml and 5 ml digestion solution with cocktail. The picture was taken three months after preparation, when color quenching had developed intensely.

Cerenkov Counting

Cerenkov counting is only applicable for high energy β-emitters and can lead to fast results since no cocktail has to be added to the solution in advance. Cerenkov radiation

is a phenomenon based on charged particles travelling trough a medium and exceeding the local speed of light. As a result bluish light is emitted and can be detected directly with the PMT. The velocity of light in a given medium with refractive index n is given as $v = c/n$. In water $n = 1.33$ which leads to a threshold β-energy of 600 keV for Cerenkov radiation to occur [26]. ^{90}Sr ($T_{1/2}$ = 28.80 years, E_{max} = 545.9 keV [29]) itself is not applicable for Cerenkov counting because its β-particles do not have sufficiently high energy, but its daughter nuclide ^{90}Y ($T_{1/2}$ = 2.67 days, E_{max} = 2278.7 keV [29]) emits high-energy β-particles which cause Cerenkov radiation [29]. Assuming that ^{90}Sr and ^{90}Y are in equilibrium, the activity of the former can be calculated via Cerenkov counting of ^{90}Y.

2.3.3 X-Ray Fluorescence Spectroscopy (XRF)

X-ray fluorescence spectroscopy is an analytical method for the detection of the elemental composition. It is a fast method and can lead to results, depending on the preparation method, within minutes. Samples in solid, powdered and liquid phase can be analyzed. Spectrometers are set in a vacuum chamber and only for the analysis of powder or liquids, the chamber is flooded with helium. Elements with low atomic number like carbon are mostly not detectable.

The main principle of XRF is the ionisation of electrons in inner atomic shells, characteristic X-ray emission by the relaxation of remaining electrons and its detection. A X-ray tube is pointed directly at the sample, the radiation gets absorbed and excites electrons in atoms. Following orbit transitions of electrons produce characteristic X-rays, which is called fluorescence radiation. These X-rays are split up according to their energy by a detection system. A wavelength dispersive system splits up the photon by their wavelength corresponding to the characteristic energy. In wavelength dispersive X-ray fluorescence (WDXRF) the emitted photons are directed through a collimator onto an analyzing crystal which diffracts them to different directions depending on their energy. After another collimator a detector is placed in a certain angle and receives incoming photons of certain wavelength. The angle is changed sequentially and the intensity of different wavelengths can be measured. Several analyzing crystals are used because different lattice spacings are needed to cover a broader measurement range [30]. Spectral data is usually presented as counts per second for different angles, 2θ.

Chapter 3

Methodology

3.1 Preparation of the Gravel Sample

In April 2023, before this study was started, building gravel was taken from the site of NES for specific investigations. The gravel was not selected according to special criteria and was available in large quantities. A regional origin is likely since ballast is usually not transferred over long distances. The material was sieved to particle sizes smaller than $5\,mm$ and $3.332\,kg$ of it was contaminated with ^{137}Cs. The object was to investigate whether this gravel could be suitable as a calibration material for a portable contamination monitor. The indented purpose was not executable and the project was put aside.

For contamination, a ^{137}Cs-gamma-standard solution in a $5\,ml$ ampoule (Eckert&Ziegler Isotope Products) was used. According to the calibration certificate the solution consisted of CsCl in $0.1\,M$ hydrogen chloride and the carrier content was $10\,\mu g$ Cs/mL on March 1st 2022. A small amount of standard solution was mixed with deionized water and $4,61\,g$ including a total activity of $68.1\,kBq$ was added to $964\,g$ of deionized water, approximately the amount of water which could be taken up by the gravel. The complete solution was dripped over the gravel and was left to air dry at room temperature. After 13 days, the gravel was dried under vacuum at $36^{\circ}C$ for one day to completely dry. Contamination and drying was performed in the same container, which can be seen in Figure 3.1.

Figure 3.1: Tin bucket filled with contaminated gravel.

Since the contamination process potentially influences the cesium distribution in the gravel in a considerable amount, the analysis of a depth profile is of great interest. In this way, deviations in the source material can be quantified and considered for further investigations. To do so the gravel was scraped off from the top in ten layers reaching from 1 to 2 cm each. Subsamples of 20 *ml* vials were taken for gamma spectroscopy.

3.2 Grain Size Analysis

To enable radiological measurements by particle size, the material was dry sieved with a vibratory sieve shaker (Analysette 3 Pro by Fritsch, Figure 3.2). The device was used with five meshes for grain diameters of 1 *mm*, 0.5 *mm*, 0.25 *mm*, 0.125 *mm* and 0.063 *mm* and therefore separated the gravel into six fractions. They are arranged by grain size in Figure 3.3. Since the gravel was already sieved to under 5 *mm* before contamination it can be assumed that the coarsest fraction contains particles from $1 - 5\,mm$ in diameter. Sieving took place for 4 minutes with a vertical magnitude of 1.5 *mm* and was repeated with a magnitude of 2 *mm*. Dry sieve analysis was preferred due to the already dry material. The column offers the possibility for wet sieving as well but this would have meant longer follow up work to dry the gravel again completely [31]. Furthermore, a loss of ^{137}Cs would have been possible. Disadvantages of dry sieve analysis might be that finer particles are not separated completely from coarse grains because adhesion makes it tricky to separate them completely.

Figure 3.2: Sieving column used for dry sieving.

Figure 3.3: Six fractions resulting from the sieving. The top right cup shows the coarsest particles descending in size to the finest particles at the bottom left.

3.2.1 Grain Size Analysis with Real Waste

To compare results of the sieve analysis of the simulated waste, a real waste sample was added to the investigations (Figure 3.4). Since reconditioning processes require samples of mostly whole drums to be evaluated in the laboratory, an extensive sample storage is available. Most of the samples there have already been analyzed for their radiological and chemical properties. The gravel that matched the contaminated gravel best, based on material structure and radionuclide inventory, was used for sieve analysis. This sample will be referred to as EB9376 from now on. Sieving analysis was conducted exactly the same way as before in Chapter 3.2, except with an additional 5 *mm* mesh because no previous sieving was performed in this case. Additionally, small amounts of the material were fired for about 18 hours at 1000°C in an ashing furnace, as described in Chapter 3.9. This enabled the production of solid glass disks for XRF spectroscopy and stored water was removed from the gravel. It is expected that also the major fraction of ^{3}H was removed.

Figure 3.4: Real radioactive waste EB9376 before sieving.

3.3 Microscopy

For a visual overview of the sieved material and the optical distinction of fractions, a microscope (Leitz, Laborlux 12) was used. It was attempted to apply only a thin layer of sieved material originating from the ^{137}Cs contaminated gravel onto the microscope slides. The microscopic analysis was performed at 5× and 10× magnification.

3.4 Sample Shredding and Homogenization

Currently, the preferred method in the local laboratories to homogenize a given material is shredding. The favorable method is grinding with a vibratory disc mill (Herzog) which leads to fine powder very fast and does not need extensive attention. Unfortunately its capacity is rather low with only approximately 30 g for each batch. Since the amount of material which is to be analyzed is usually larger either the process has to be repeated several times or a planetary ball mill is used instead. The local planetary ball mill (Retsch, PM 100) allows pulverization of up to 125 ml for each batch. A disadvantage is the produced heat due to it's high centrifugal forces and friction, which makes it necessary to let the jar cool down for at least several hours to avoid explosion due to the high pressure.

Powdered samples are crucial not only for representative reasons, but also for sample preparation itself, like for XRF. All three XRF measurement techniques investigated in this study require powdered material, i.e. loose powder, pressed powder and glass disks.

Beside the sample preparation, the aim of this investigation was to show that grinding leads to greater homogenization of samples and higher representativity of subsamples. Therefore, ten subsamples of 20 ml vials taken from the upper and lower halves of the container and previously measured with gamma spectroscopy before to quantify inhomogeneities were mixed together. The samples still contained coarse particles, when mixed. The planetary ball mill was then used to grind the entire mixture, which was separated into subsamples to determine the uniformity of activity concentration with gamma spectroscopy.

3.5 Gamma Spectroscopy

The gamma detector (Canberra), which was used for the entire study, is a high purity germanium semiconductor detector (HPGe) with an active diameter of 60 mm and 58 cm^3 of active volume and a 2 keV resolution at the 1332.5 keV ^{60}Co photo peak [32]. The crystal is shielded by lead and copper layers and its window consists of carbon epoxy. The system is cooled with liquid nitrogen to minimize thermal noise.

All samples were measured either in 500 ml cups, see Figure 3.3, or in 20 ml polyethylene LSC vials, see Figure 2.3. The 500 ml cups are not specifically shaped for gamma spectroscopy measurements because their bottom is curved and not of same thickness at all points. This means it is hard to define the exact geometry of the cup. However, the containers were implemented all over the facility of NES because they are more cost efficient and easy to handle between different facilities on the site. The LSC vials do have less anomalies in their surface and represent a more suitable geometry. Solid glass disks prepared for XRF analysis, shown in figure 3.10, were directly measured with a petri dish of known geometry.

The spectra visualization and evaluation was done with Genie2000 and sample geometry was modeled with an isocs geometry editor. The nuclide data base was adapted to the contents of the samples in order to avoid false isotope assignments. Gamma emitters are characterized by their discrete energies and can therefore be assigned to detected photo peaks. The radionuclide ^{137}Cs, which is omnipresent in this study, is a β^--emitter and after its decay to ^{137m}Ba a characteristic gamma ray at 661.66 keV is emitted [8].

For a reliable evaluation of radioactive waste it is important to gain knowledge about the radiological content of the sample. Since many radionuclides overlap each other with their photo peaks, it is of great advantage to work with an adapted nuclide data base where only potentially occurring radionuclides are present. Therefore, typical gamma sepctra of uncontaminated soil were recorded for preliminary tests, and an example spectrum can be seen below in Figure 3.5. It shows peaks of nuclides of all three natural decay chains. Usual radionuclides included in natural decay chains are present and could be quantified as matching the range in which naturally occuring activity concentrations lie. These values are strongly dependent on the region but mean values for soil in Europe are located on the order of 35 Bq/kg [33]. Many nuclides are in equilibrium with each other as expected in undisturbed stones. This gravel material is mineralogically similar to the sample contaminated with Cs-137 and one can assume to find similar activity concentrations of natural radionuclides in the material through the following study. The measurement was carried out for 72 hours to acquire sufficient detections for these low activity concentrations.

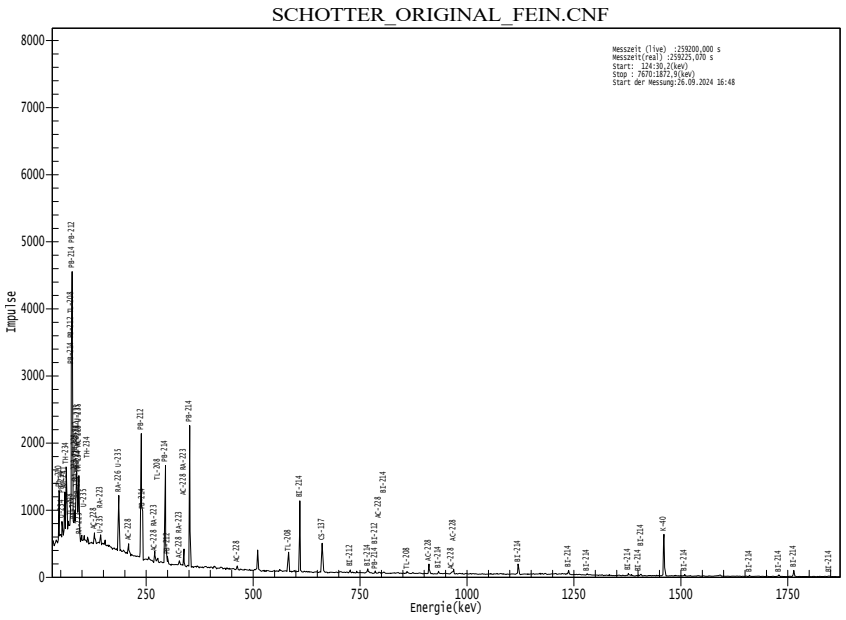

Figure 3.5: Spectrum of not contaminated building gravel from the site. Measuring time was 72 hours to acquire sufficient decay detections for low activity concentrations. Radionuclides belonging to the natural decay chains starting with ^{232}Th, ^{235}U and ^{238}U can be seen.

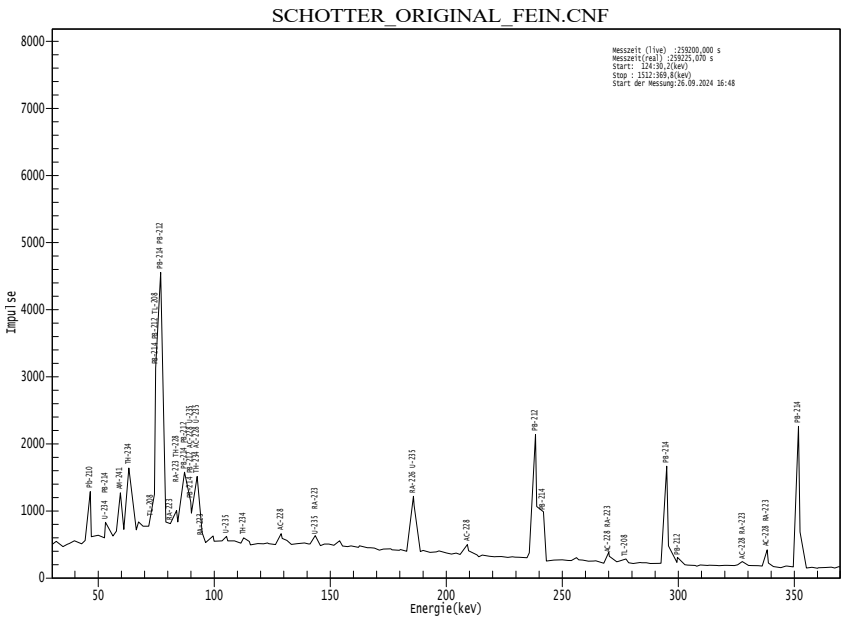

Figure 3.6: Detail of Figure 3.5 with the lowest energy photo peaks up to 360 keV.

3.6 Liquid Scintillation Counting (LSC)

Since the radionuclide inventory of EB9376 is not completely described by gamma spectroscopy, LSC was carried out additionally. About 50 *g* of the material was ground with the disc mill to obtain a representative sample. For further results of radionuclides in the low energy range, LSC was carried out with 4.46 *g* of fired sample material as well. Comparison of the unfired with the fired sample spectrum were conducted in order to evaluate ^{3}H and ^{241}Pu.

First a chemical digestion was performed in order to dissolve radionuclides from the solid particles. 15.67 *g* of powdered sample material was mixed with 100 *ml* deionised water and 50 *ml* of nitric acid and heated up on a hot plate. Nitric acid was added until carbon dioxide release because of carbonate in the sample had stopped. A total of 125 *ml* of nitric acid was added. The solution was kept at temperature for several hours before it was turned off. A second method was used with a microwave digestion system (Anton Paar, Multiwave 5000), which simplified the process of digestion and took 20 minutes to be completed due to its higher temperature and pressure compared to the first method with the beaker and hot plate. A disadvantage was the small amount of sample material of 3 *g*, which can be introduced in one sample holder. 5 *g* of deionised water and 5 *g* of nitric acid were added before digestion was started. The unfired sample was processed according to the first method including the beaker. The digestion of the fired sample was done with the microwave system.

Further preparation was the same for both methods. The solution was transferred to a funnel where the liquid phase passed a glass microfibre filter (VWR) which held back particles smaller than 1.5 μm. The resulting residues of the unfired sample was put aside to dry by air and was analysed by gamma spectroscopy to evaluate the digestion yield. The residue of the fired sample was dried in a vacuum drying cabinet (Thermo, VT 6025) linked to a diaphragm vacuum pump (Vacuubrand) for one day at 80*C* to ensure complete drieness before gamma spectroscopy. The resulting clear solution was prepared for several measurements in the liquid scintillation spectrometer. First, pure solution was filled in two 20 *ml* vials, where one was measured in the gamma detector in order to fill in necessary gamma activity of the sample, when evaluating the LSC spectrum. The second vial was measured for its Cerenkov radiation, which is used to determine ^{90}Sr activtiy concentration by the high energy β-particles of ^{90}Y. Since the solution was clear and color quenching was not expected, it was measured without further dilution. The low activities of the samples made it even more important to keep the radionuclides' concentrations as high as possible. For the actual LSC, a third vial was prepared with 1 *ml* of filtered digestion solution, 4 *ml* of deionised water and 15 *ml* of a special LSC Cocktail (Ultima Gold AB) and was measured in $\alpha\beta$-mode of the detector system. Both modes, Cerenkov and $\alpha\beta$, were carried out in the ultra low level liquid scintillation spectrometer (1220 Quantulus). A higher ratio than 1 *ml* of digestion solution mixed with the cocktail meant higher quenching effects and were unfavorable regarding spectra evaluation.

3.7 Sr-90 Separation

To obtain clear results regarding ^{90}Sr activity concentrations in the samples, which had been analyzed with LSC before, chemical separation was performed. Interfering radionuclides were removed and single ^{90}Sr spectra with ingrowing ^{90}Y were recorded with LSC. The results were compared to those obtained by LSC with the sample before separation.

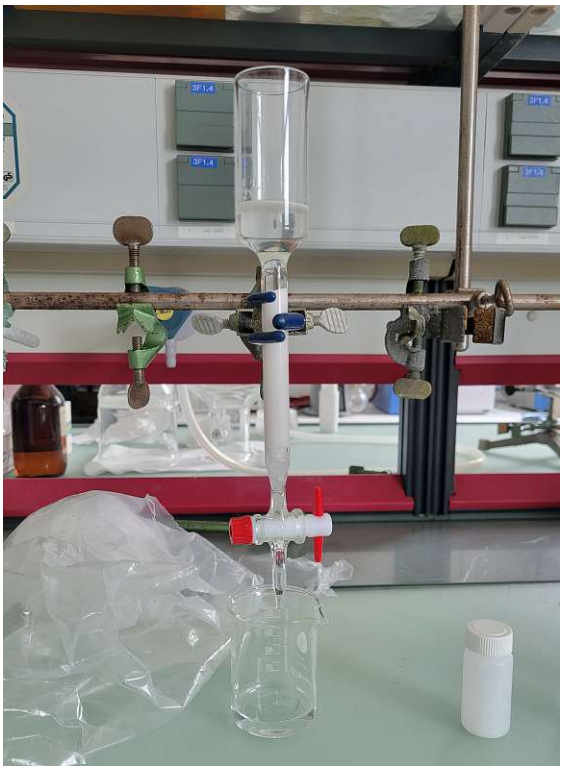

Figure 3.7: Separation column filled with quartz wool, glass fiber filter and resin. The picture shows the column with introduced nitric acid.

To separate strontium from other elements, a well-defined routine previously established at NES was used, which starts with a digestion solution of the analyte. The solution obtained by digestion of the unfired material, which has already been used for LCS measurements, was processed. Separation itself took place in a glass column filled with quartz wool and a glass fiber filter. For further set up preparation, 3 g of a strontium resin were mixed with a small amount of deionized water and poured into the column. This special strontium resin (TRISKEM) contains a crown-ether which works as extractant for strontium. Cavities in the crown-ether adsorb strontium under certain circumstances very well. For high concentrations of nitric acid, i.e., 3M to 8M nitric acid, the resin shows great affinity of strontium whereas the affinity for almost all other alkaline and alkaline

earth elements is non-existing [34]. Furthermore, 30 *ml* of digestion solution were mixed with 1 *ml* of a strontium nitrate solution to prepare the so called feed solution. Separation itself is a rather time-consuming process because all substances drip trough a narrow neck containing the quartz wool and the resin. First, the column filled by resin was rinsed with 30 *ml* of 8 M nitric acid before the feed solution was poured in. When the feed had dripped through, another 50 *ml* of 8 M nitric acid were added continuously. It was assumed that the whole strontium was concentrated in the column at this point. The transition phase, which changed the acidity in the column, was carried out with 12 *ml* of 0.05 M nitric acid. Then, the acidity in the column had changed and strontium was released by the crown-ether. When dripping had stopped, 30 *ml* more of 0.05 M nitric acid was added, the strontium was extracted from the column and caught in a beaker. To achieve higher strontium concentration the eluate was evaporated to dryness by a heat lamp for approximately two hours. The residue was dissolved in 6 *ml* of 0,05 N nitric acid and processed for LSC and ICP measurements. The strontium yield was investigated with ICP by comparison of the feed solution and the eluate.

3.8 Deconvolution of LSC Spectra

Most samples include several β-emitters which leads to diverse LSC spectra. To avoid nuclide specific chemical separation, an established evaluation routine is used, which is based on the suggested methods explained in [35]. In the following, this routine is explained and illustrated using an example spectrum of a recent waste sample.

The raw data was read into a prepared excel file where an up to date background was subtracted. The resulting spectrum of the β-channel was smoothed over 20 channels and a combined ^{90}Sr and ^{90}Y standard spectrum was adapted to the high-energy edge, as seen in Figure 3.8a. At this point, the counts of ^{90}Sr and ^{90}Y were determined and the activity was calculated. It was assumed that both radionuclides are in equilibrium and therefore the ^{90}Sr activity accounts for half of the total activity of the fitting curve. From experience in waste characterization, it was assumed that the remaining spectrum consists of counts of ^{137}Cs and ^{241}Pu mainly (see red line in Figure 3.8b). The huge signal probably from ^{137}Cs was cut off the low-energy spectra with a cubic spline. The cubic spline is supposed to continue the ^{137}Cs spectrum to lower energies correctly and expose the remaining ^{241}Pu spectrum (see yellow line in Figure 3.8b). Depending on the sample, a slight signal of ^{63}Ni is possible. In the evaluation a signal of ^{63}Ni close to the high-energy edge of ^{241}Pu was observed. By subtraction of the spectrum with a standard spectrum, like it was done with ^{90}Sr and ^{90}Y, quantification of ^{63}Ni activity concentration was carried out. The remaining peak gets usually assigned to ^{241}Pu, but the resulting activity concentration was too high compared to the known activity of ^{241}Am measured by gamma spectroscopy and an indication for ^{3}H was given.

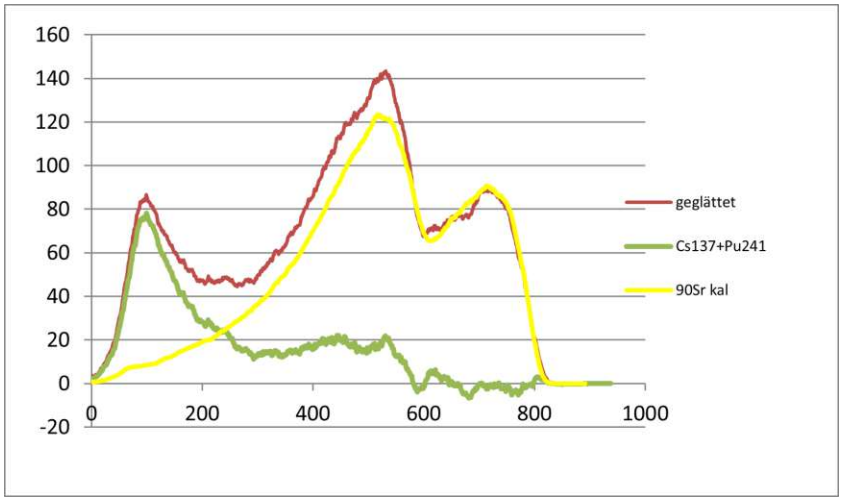

(a) The red line represents the smoothed source spectrum. The ^{90}Sr and ^{90}Y standard curve in yellow is adapted to the red curve manually. After subtraction the resulting spectrum is depicted in green.

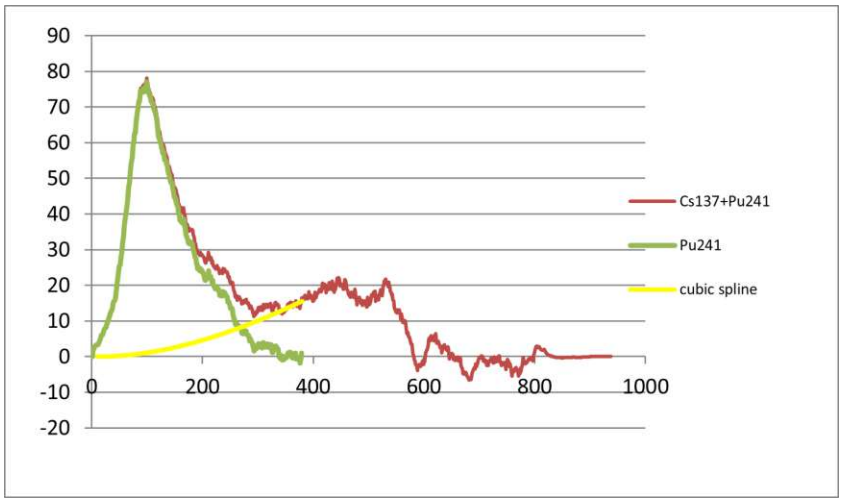

(b) Taking the obtained data from the green line above this graph shows the spectrum in red. The cubic spline in yellow is adapted to mimic the ^{137}Cs count decrease. The green line is assumed to originate only from ^{241}Pu.

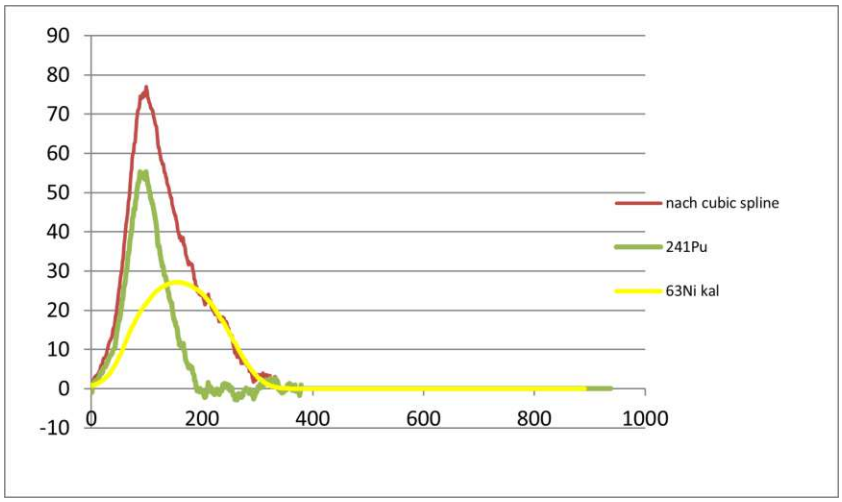

(c) Standard spectrum of ^{63}Ni is subtracted from the remaining spectrum.

Figure 3.8: Original graphs from the evaluation routine. The total counts are depicted on the vertical axis and the channel number on the horizontal axis. Raw data is smoothed over 20 channels.

For this study, LSC measurements and spectra deconvolution were performed three times on the same sample in order to evaluate deviations within the routine and to show reproducibility.

After strontium separation, data analysis was performed differently. Multiple measurements were repeated over the days after separation until equilibrium was reached after approximately ten days. Right after the separation, only ^{90}Sr was detectable but since there were time steps between separation and actual measurement, pure ^{90}Sr spectra could not be detected in the application. Therefore a kinetic analysis of the ingrowing ^{90}Y was performed including quantification of activity concentration.

3.9 X-ray Fluorescence Spectroscopy (XRF)

An XRF device (Panalytical Axios max advanced) and the associated software were used for the investigation of three different sample types and the comparison of elemental composition with ^{137}Cs activity concentration. All three sample preparation techniques, loose powder, pressed pwoder and solid glass disks, were applied for the first measurement series, i.e., samples from the depth profile, and compared to each other. Subsequent XRF measurements were only done on glass disks, which turned out to be the most precise technique.

Measurements with loose powder required the least effort and preparation was done within a few minutes. Ground sample material was poured into a plastic cup with foil stretched around the bottom of the cup to a height of approximately $5\,mm$.The measurement chamber had to be flooded with helium to prevent issues of contamination by the powder.

Pressed powder pellets were prepared with ground sample powder mixed with a binder to assure shape and mechanical stability during compression and after. $8\,g$ of sample material and $2\,g$ of wax (Hoechst wax C micropowder) were combined and adequately mixed with a shaker (IKA-Labortechnik, Vibrofix VF1) to ensure homogeneous pressing conditions. The mixture was poured into a special aluminum cup and compressed with a high pressure press (ToniPact 3000) at $250\,kN$. During compression a diaphragm vacuum pump (Vacuubrand) was connected to remove air from the sample. The resulting pellet required careful handling but was stable enough for the following XRF measurements.

The most time-consuming, yet most favorable, form of sample preparation for XRF are solid glass disks. Since the gravel contained a certain amount of carbon in different chemical forms such as calcium carbonate, the material had to be fired before melting. Calcium carbonate would have led to the formation of bubbles in the glass during the melting process. To calculate the loss on ignition (LOI), the empty ceramic crucibles' weight was documented and approximately $5\,g$ of sample powder was added. Ignition took place over night for about 18 hours at $1000^{\circ}C$ in an ashing furnace (Carbolite Gero). The furnace was unloaded a couple of hours after switching it off, when temperature had already dropped. Afterwards, the ceramic crucibles were transferred to a desiccator until

they could be handled manually. After weighing for the LOI, 1 *g* of sample material was transferred to a platinum crucible for melting and flux was added to enhance melting properties. Therefore, 5 *g* of flux (Spectromelt A 12), a mix of di-lithium tetraborate and lithium metaborate, and 50 *mg* of Lithium bromide hydrate were added to the sample and stirred. The prepared platinum crucible was loaded in the holder of the fusion instrument (Claisse LeNeo) and the required fusion program was started. A viewing window allowed insight into the pouring (Figure 3.9) and cooling process. The glass disks were placed in the XRF device and measured one after another (Figure 3.10).

Figure 3.9: Pouring of the melted glass into the mold.

Figure 3.10: Glass disks in the XRF device. The darkening of irradiated glass disks (bottom) is visible. Not yet irradiated disks (top) were almost transparent.

3.10 ICP-OES

Inductively coupled plasma optical emission spectroscopy (ICP-OES) was applied to determine the separation yield for strontium. For this purpose, approximately 1 *ml* of feed and separation solution were taken each and diluted with deionized water to lower the elemental concentration and to improve measurement conditions. In the ICP-OES device, part of the sample solution was taken up with a thin tube and introduced into an argon plasma with a nebulizer system. In the plasma, part of the strontium atoms were ionized and electron excitation and relaxation causes characteristic photons. Three

characteristic energies with wavelength of 346.446 *nm*, 407.771 *nm* and 421.552 *nm* contribute to strontium content detection. Standard solutions were measured before as well.

Chapter 4

Results

4.1 Influence of Contamination Method on Cesium Distribution

The contamination method, which involved dripping cesium solution from above onto the gravel, led to significant deviations in ^{137}Cs activity concentrations, as shown in Figure 4.1. The highest activity concentrations were found in the upper layers. Samples taken from the lower half of the bucket showed the lowest activity concentrations. However, the measurement results did not show a monotonically decreasing behavior and the sample taken from the bottom was quantified with an activity concentration significantly above the average of 20.43 Bq/g. Lowest value was quantified with 46.65 % below and the highest value with 42.92 % above average activity concentration.

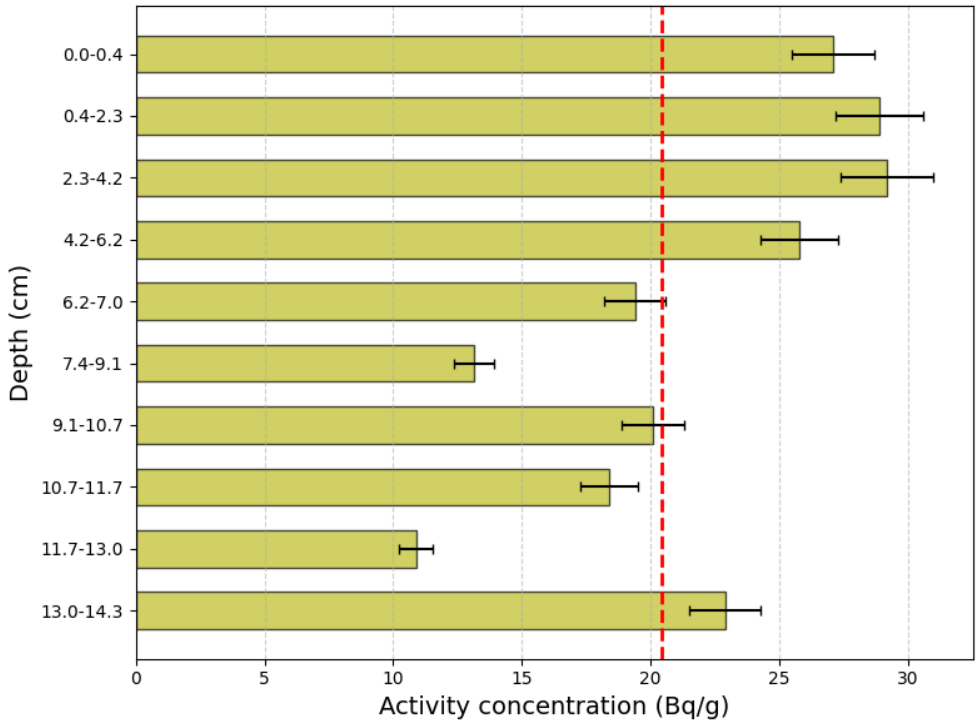

Figure 4.1: Activity concentrations of ^{137}Cs measured for ten different depth intervals. The red vertical line represents the average activity concentration that was aimed for in the original experiment, which is 20.43 Bq/g.

4.2 Sieve Analysis Results

To enhance the understanding of the gravel fractions first on a visual basis, the four smallest fractions were observed through the microscope. Images of these, captured through the objective, are presented in Figure 4.2. Not only can particles with different grain sizes be seen, ranging between the mesh grids, but also relatively fine material can be observed in between. Due to dry sieving not all particles were divided up completely and some of the smallest particles were found to be adhering to the larger particles. Apparent are different optical properties of minerals within the fractions. The smallest fraction 4.2d, which consisted of the bottom layer of the sieving column, mostly consisted of conglomerates rather than separated particles and single minerals are less distinguishable.

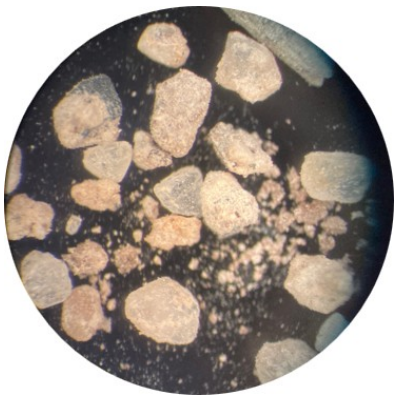

(a) $500 - 250\,\mu m$, $5\times$ objective

(b) $250 - 125\,\mu m$, $5\times$ objective

(c) $125 - 63\,\mu m$, $10\times$ objective

(d) $< 63\,\mu m$, $10\times$ objective

Figure 4.2: Images of the four smallest fractions taken through the microscope. Mind that two different objectives were used. Dusty particles, visible on the pictures, were not fully separated from coarse particles through dry sieving.

Following the sieving process, the resulting mass and volume distribution were evaluated and can be seen in Figures 4.3a and 4.3b. Both quantities show a similar distribution, where the majority consists of the fraction of particles with the largest size.

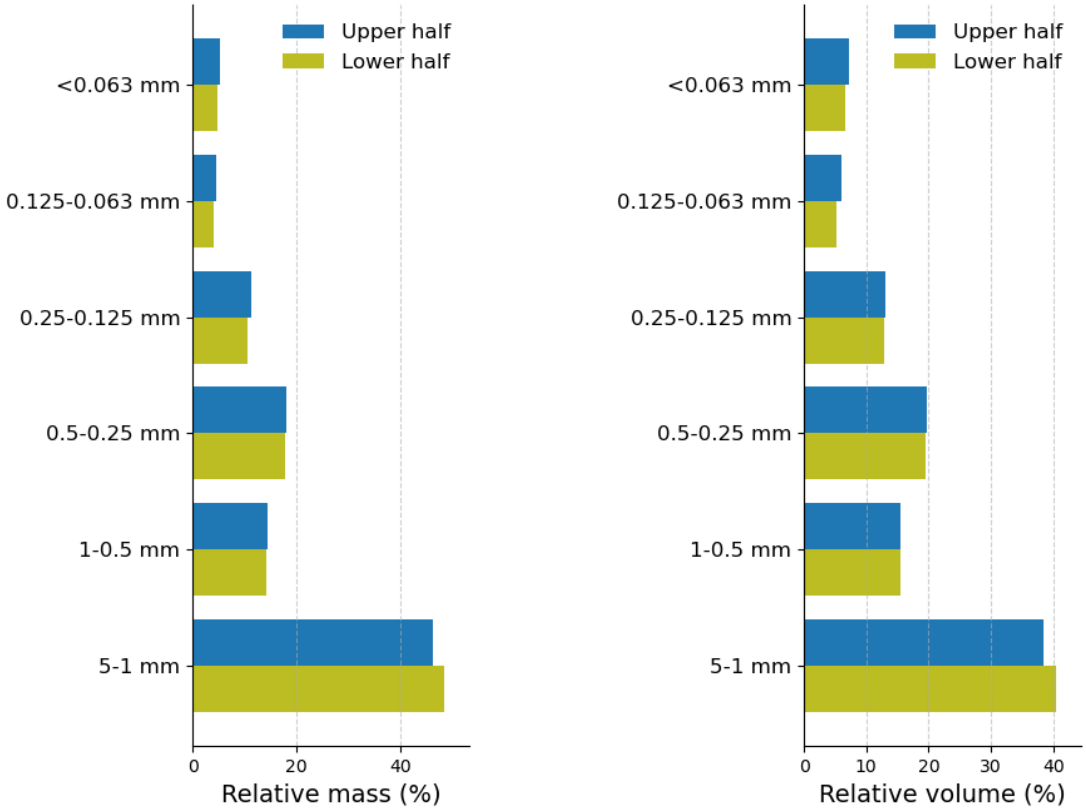

(a) Relative mass distribution of sieved fractions.

(b) Relative volume distribution of sieved fractions.

Figure 4.3: Mass and volume distribution of the gravel after sieving. The upper and lower halves are shown side by side but show similar behavior.

The ^{137}Cs activity concentration was measured for both, lower and upper half for each fraction and is depicted in Figure 4.4.

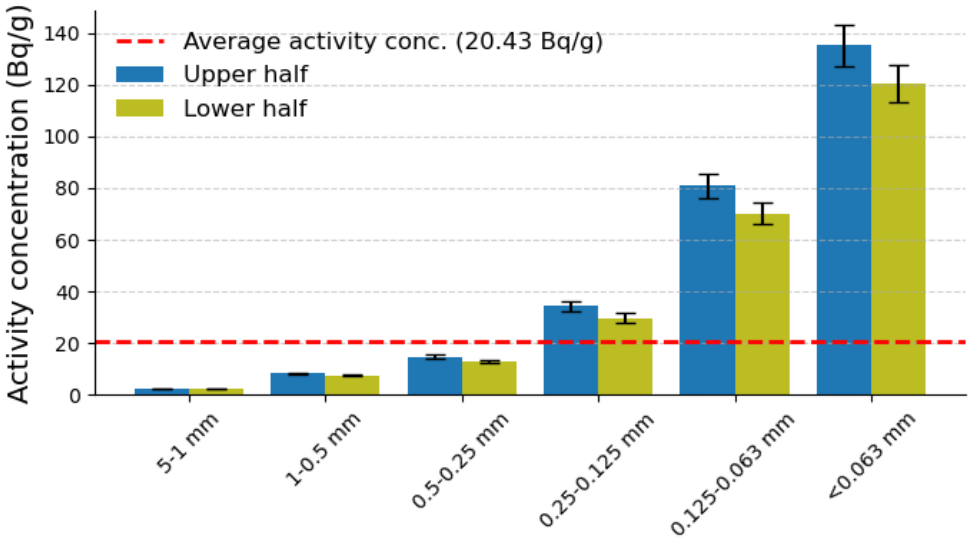

Figure 4.4: Activity concentrations of ^{137}Cs for each fraction. The red horizontal line indicates the mean activity concentration of the whole gravel. These $20.4 Bq/g$ were aimed for during the original contamination of the sample. Particles with the largest diameter show comparably low activity concentrations and lie below the exemption limit for ^{137}Cs, which is $10 Bq/g$ [36].

In order to enable further comparisons between activity concentrations and fractions, a mean particle size was assumed. In Figure 4.5 the decrease of activity concentration with an increasing particle diameter can be seen. Based on this mean particle diameter, a specific surface area for each fraction was calculated. This was then compared to the ^{137}Cs activity concentration as Figure 4.6 visualizes the influence of the specific surface area on the measured ^{137}Cs activity concentration. For larger particles, a linear increase of activity concentration with surface area is visible.

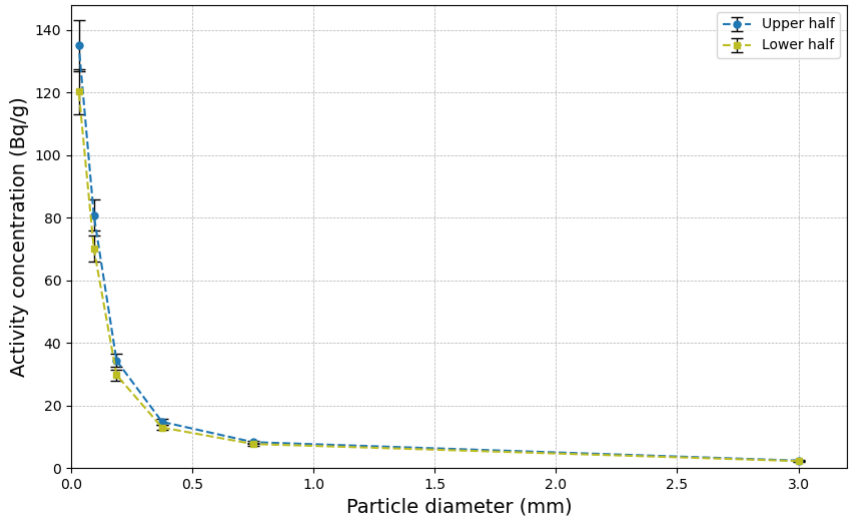

Figure 4.5: Assumed mean particle diameter of each fraction compared to its measured ^{137}Cs activity concentration.

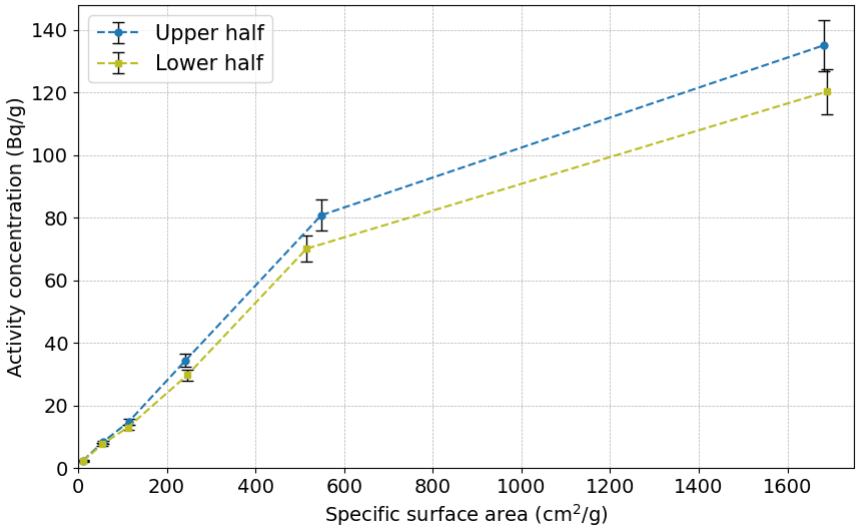

Figure 4.6: Calculated specific surface area of each fraction compared to its measured ^{137}Cs activity concentration.

4.2.1 Sieve Analysis of Real Waste EB9376

As mentioned before, a real waste, which was available for further analysis, was sieved and analyzed according to previous procedures. Mass and volume distributions of this material, depicted in Figure 4.7 show similar results compared to the simulate. The activity concentrations of the three main radionuclides that have been identified in the inventory of the waste are shown in Figure 4.8. As observed for the waste simulate (Figure 4.4) the activity concentrations for coarse particles are the lowest. Values are abruptly increasing for particles smaller than 1 mm and continue to rise, except for ^{137}Cs, for smaller particles continuously.

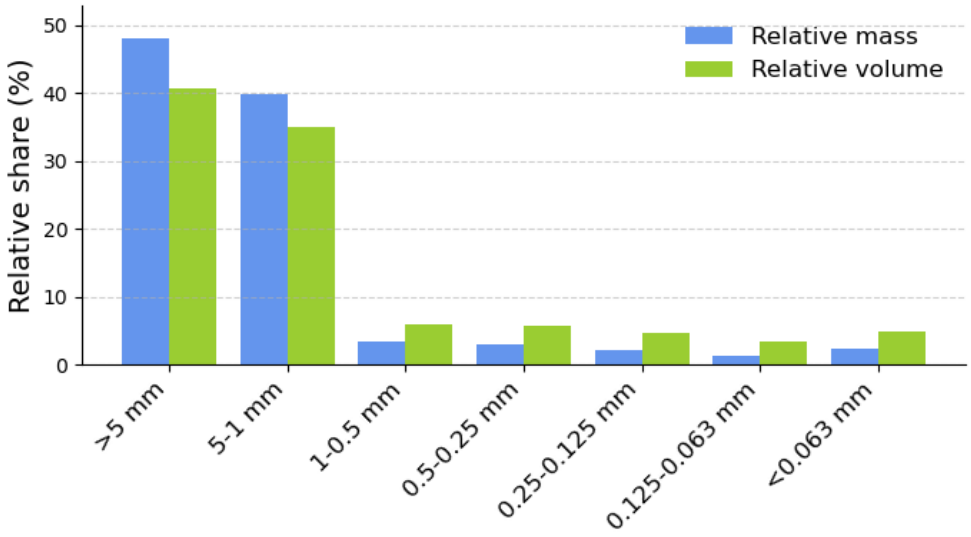

Figure 4.7: Relative mass and volume distribution of sieved fractions of EB9376. Mind the additional fraction with particles above 5 *mm*. The waste simulate was contaminated after sieving with a mesh of 5 *mm* and did therefore not consist of particles larger than 5 *mm*.

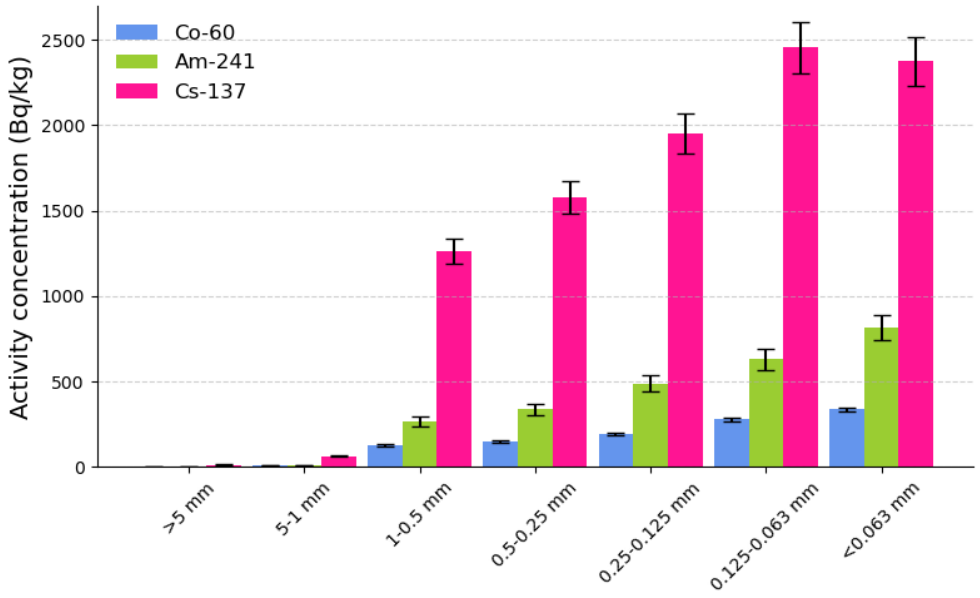

Figure 4.8: Activity concentrations of each fraction of EB9376. Thresholds for release are above the detected maximum activity concentration and not depicted in the graph.

4.3 Eliminating Inhomogeneities within the Gravel

Random samples from the upper and lower half of the original material, which were assumed to contain identical activity concentrations, show significant deviations to each other. This fundamental gap in activity concentration between upper and lower half can be seen in Figure 4.4 as well. Within both halfs the deviation of subsamples is less as can be seen in Figure 4.9. From these ten subsamples, which were mixed and later ground, four subsamples were taken and measured for their activity concentration. The results are shown in Figure 4.10.

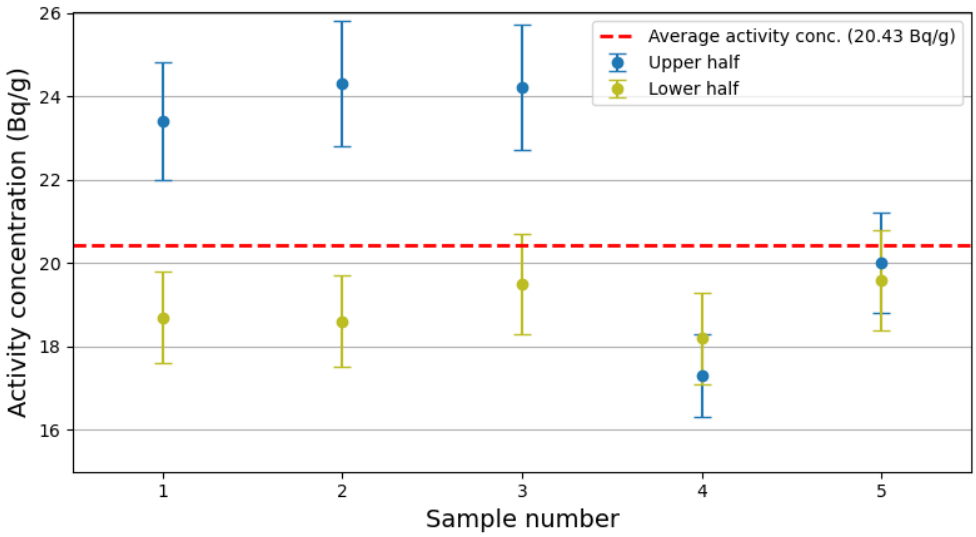

Figure 4.9: Samples taken from upper (blue) and lower (green) half of the original container and measured in 20 ml vials with gamma spectroscopy. Most of them do significantly differ from the intended average ^{137}Cs activity concentration of 20.43Bq/g. Sample number four and five of the upper half show the presence of outliers.

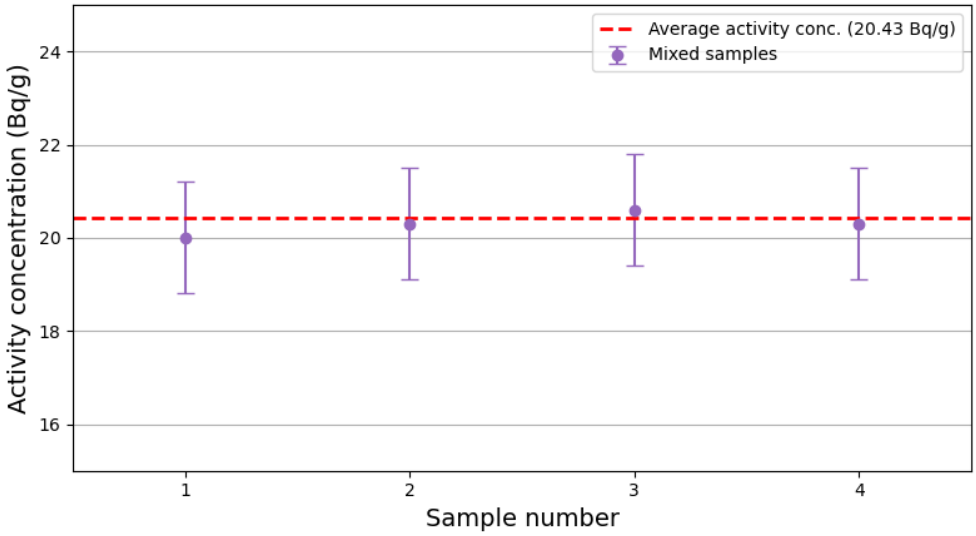

Figure 4.10: Repeated measurements of subsamples in 20 ml vials. Samples of Figure 4.9 had been mixed and ground. The four samples, taken from this mixture, lie on the average ^{137}Cs activity concentration of the gravel simulate.

4.4 Beta Emitters in EB9376

Cerenkov counting was repeated three times each with the pure digestion solution of the unfired and fired material. All other activity concentrations of the observed radionuclides were quantified through the evaluation routine described above. Results for the unfired sample can be seen in table 4.1.

	Activity concentration (Bq/g)				
	1	2	3	mean	std dev
^{90}Sr CER	0.943	0.994	0.981	0.973	0.027
^{90}Sr LSC	0.929	0.990	0.935	0.952	0.034
^{63}Ni	1.54	1.37	1.29	1.40	0.13

Table 4.1: The results for ^{90}Sr were obtained via Cerenkov counting and LSC, and for ^{63}Ni via LSC with the evaluation routine 3.8, which has previously been described. The activity concentration of ^{241}Pu was overestimated with the detected spectrum and is not listed here.

The spectra deconvolution produced far too high results for ^{241}Pu. Due to similar β energies and the known occurrence of ^{3}H in radioactive wastes, it was assumed that both ^{3}H and ^{241}Pu were present in the sample and contributed to counts in the low β energy region below $20.8\,keV$. To quantify the activity concentrations of ^{241}Pu, a fired sample was measured as well in order to eliminate ^{3}H traces in the samples. The results for the fired sample are shown in table 4.2.

	Activity concentration (Bq/g)				
	1	2	3	mean	std dev
^{90}Sr CER	0.740	0.760	0.800	0.767	0.031
^{90}Sr LSC	0.8151	0.8232	0.8117	0.8167	0.0057
^{63}Ni	0.827	0.811	0.780	0.806	0.024
^{241}Pu	0.343	0.312	0.269	0.308	0.037

Table 4.2: The results of the second measurement series with fired sample material. Except for the Cerenkov counting for the first ^{90}Sr activity concentration, all results were obtained applying the evaluation routine described above (see 3.8).

The activity concentration for ^{3}H was estimated through the count difference in the low energy range of spectra obtained from fired and unfired samples. ^{3}H activity concentration was calculated as $(3.67 \pm 0.41)\,Bq/g$.

4.4.1 Digestion Yield

Activity concentrations for γ emitters like ^{137}Cs and ^{241}Am of the digestion solution were quantified by gamma spectroscopy for the LSC evaluation routine. However, digestion yield and residual yield are determined for a better understanding of the behavior of radionuclides during digestion. The results are summarized in table 4.3. Activity concentrations of ^{60}Co could not be quantified in the digestion solution of the unfired and fired sample or in the residual of the unfired sample. The values were below the detection limit, possibly because only 20 ml of the total digestion solution (approximately 200 ml) were measured.

		Activity concentration (Bq/kg)			Total activity (Bq)		
	Weight (g)	^{137}Cs	^{241}Am	^{60}Co	^{137}Cs	^{241}Am	^{60}Co
Solid n.f.	15.665	275 ±17	58.7 ±6.1	29.24 ±1.5	4.30	0.92	0.46
Digestion	15.665	200 ±25	55.9 ±12	0	3.13	0.88	0
Yield		72.7%	95.3%	0.0%	72.7%	95.3%	0.0%
Residual	4.1315	567 ±35	0	0	2.34	0	0
Solid f.	4.4585	259 ±19	83.6 ±9.9	47.0 ±8.3	1.15	0.37	0.21
Digestion	4.4585	114 ±21	65 ±12	0	0.51	0.29	0
Yield		44.0%	78.2%	0%	44.0%	78.2%	0%
Residual	2.8871	236 ±15	31.5 ±3.5	12.4 ±2.6	0.68	0.09	0.04

Table 4.3: Activity concentrations and total activities of the most relevant radionuclides found in different treatment conditions. Upper table shows results of the solid ground and unfired powder (solid n.f.), the digestion solution and the residual material after digestion. Identical for lower table which shows results of the ground and fired sample (solid f.). Values with uncertainties were measured with gamma spectroscopy. Total activities show a comparison of the recovery rates for digestion solution and the residual. Digestion yield is related to the initial values of the powdered solid material. The high cesium retention indicates that cesium is not just adsorbed on the surface but strongly bound to the matrix.

4.4.2 Separation of Strontium

For the strontium separation it was most important to remove other radionuclides i.e. ^{241}Pu, ^{63}Ni and ^{137}Cs seen in the LSC spectrum from the sample. The separation successfully led to a pure ^{90}Sr solution or strictly saying to ^{90}Sr and ^{90}Y, since ^{90}Y is growing in over hours and days after separation. The separation yield is 98.96 % and was analyzed by ICP-OES, so practically the whole strontium was separated and collected successfully. The separation solution was measured with LSC several times until day 16 after separation. Through extrapolation of the single results with ingrowing ^{90}Y the activity in equilibrium was calculated. Assuming that ^{90}Sr and ^{90}Y contribute to the total counts equally in

equilibrium, half of it represents ^{90}Sr counts. In Figure 4.11 the increasing counts per second over days and the approach to an equilibrium can be seen. The measured counts per second of this parent-daughter system obey the following equation, if the initial count rate of ^{90}Y equals zero. The term $\exp(-\lambda_Y t)$ approaches zero for large times, which means that ^{90}Sr and ^{90}Y then contribute to the count rate equally, in total with $2cps_{Sr}$. A change in the count rate of ^{90}Sr can be neglected in this context. The decay is given by $\lambda_Y = \frac{ln(2)}{T_{1/2,Y}} = \frac{ln(2)}{230.55 \cdot 10^3\,s} = 3.007 \cdot 10^{-6}\,s^{-1}$ [29].

$$cps(t) = 2cps_{Sr} - cps_{Sr} \cdot \exp(-\lambda_Y t)$$

In order to obtain a linear regression, the counts per second were plotted as a function of $\exp(-\lambda_Y t)$, which is shown in Figure 4.12.

After including the actual material weight in the sample, the ^{90}Sr activity quantifies as $0.8010 \pm 0.0093 Bq/g$.

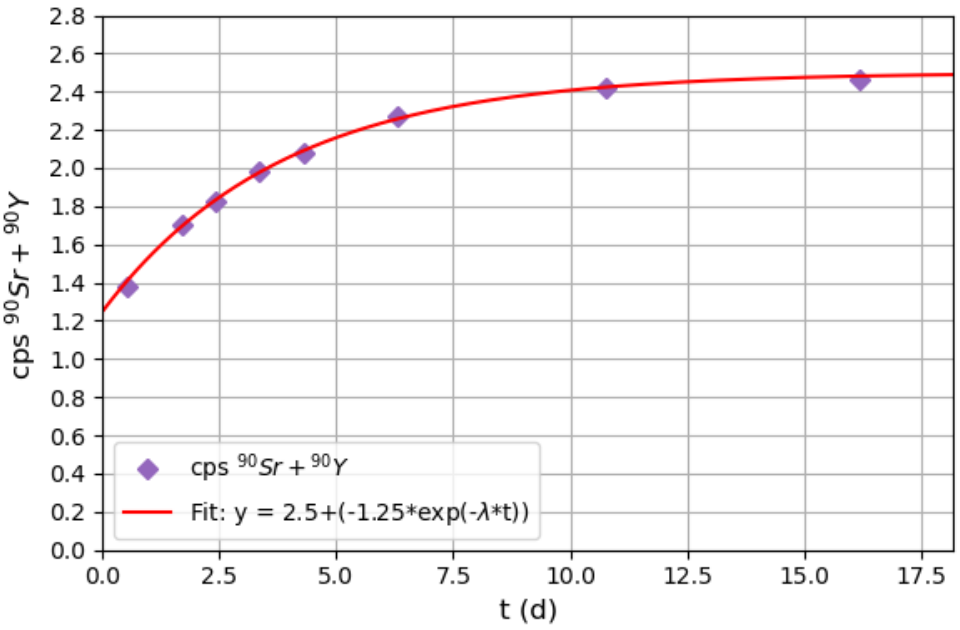

Figure 4.11: Total counts per second for ^{90}Sr and ^{90}Y over time. The intersect of the fit with the y axis at initial time represents cps of ^{90}Sr.

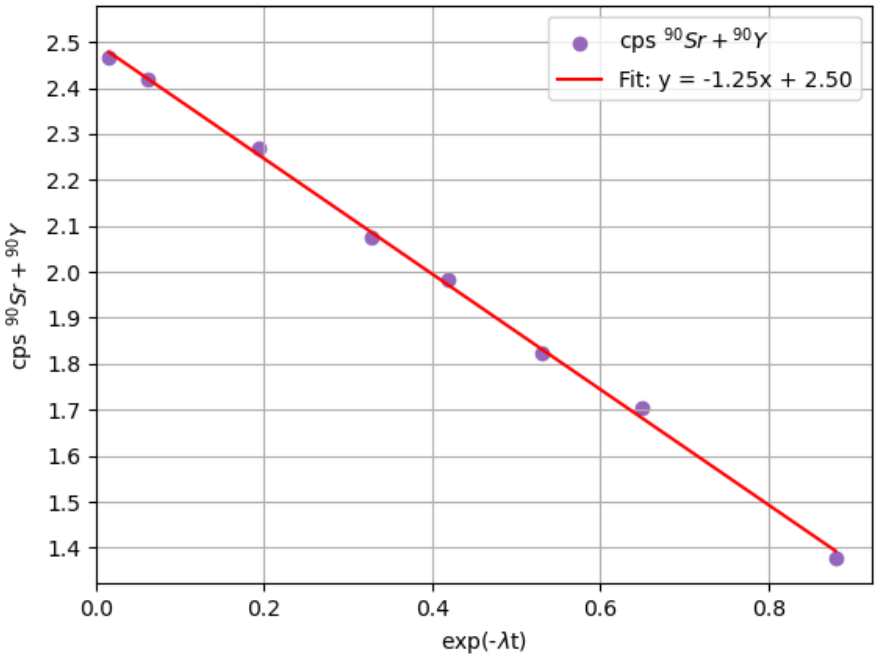

Figure 4.12: Quantification of total counts per second for ^{90}Sr and ^{90}Y through intercept of linear fit with y-axis. The decay constant is $\lambda = 0.26$ for ^{90}Y. The exponential term $\exp(-\lambda_Y t)$ tends to zero for large t, i.e. in equilibrium, and at initial time $t = 0$ it equals 1. Last measurement took place 16.29 d after separation.

4.5 Activity Concentration vs. Elemental Composition

The hypothesis that the activity concentration of ^{137}Cs is related to the elemental composition of the sample has long been investigated by XRF. All samples from the depth profile and sieving investigations were prepared as glass beads for XRF analysis. Their elemental compositions were compared to their ^{137}Cs activity concentrations.

For samples originating from the depth profile no connection of these two quantities could be determined. Elemental concentrations of the four most abundant oxides can be seen in Figure 4.13. Nevertheless, the comparison of the three different methods for XRF sample preparation, as it was carried out with all samples from the depth profile, was investigated in detail and can be seen in the appendix.

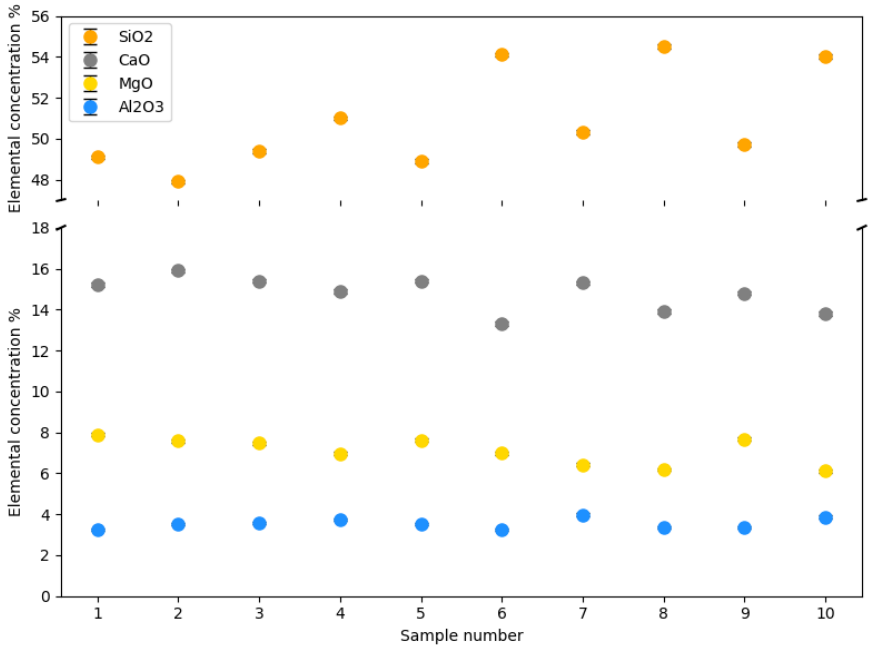

Figure 4.13: Elemental concentrations for the most abundant elements in samples of the depth profile. Depth increases from left to right. Elements are presented as oxides.

Investigations on samples of the sieved gravel did not lead to significant correlations between elemental concentrations and ^{137}Cs either except for one oxide.

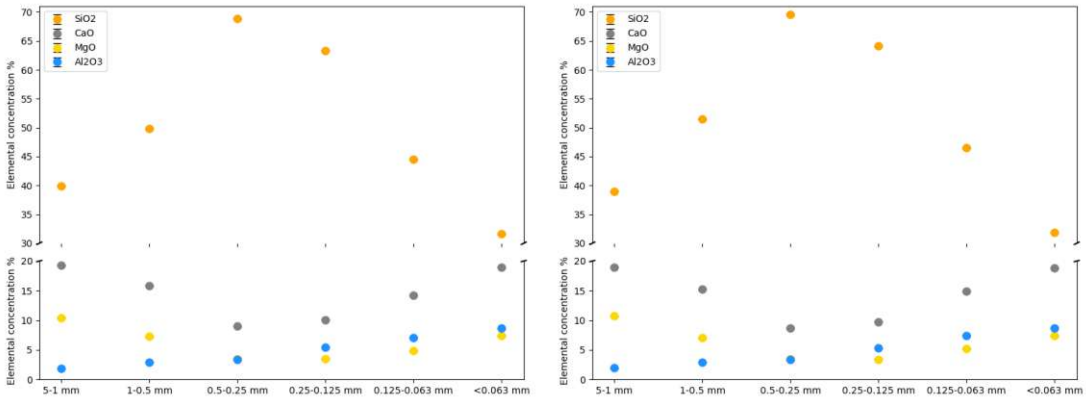

(a) The results for samples from upper half. (b) The results for samples from lower half.

Figure 4.14: Elemental concentrations for the most abundant elements of the sieved fractions of upper half (4.14a) and lower half (4.14b) of the original container. In both graphs the different compositions of each fraction are visible. The results are almost identical for upper and lower half. Compared with the ^{137}Cs activity concentration of these fractions in Figure 4.4 there is no apparent connection.

Aluminum oxide concentrations increase for smaller particle sizes. Al_2O_3 is mainly associated with clay minerals.

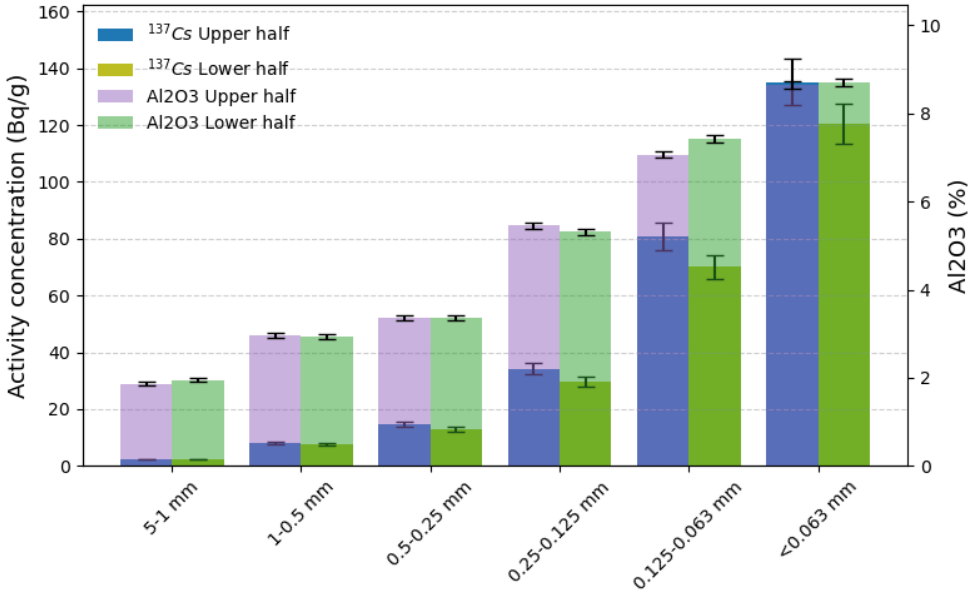

Figure 4.15: Al_2O_3 concentration compared to ^{137}Cs activity concentration in each fraction.

Chapter 5

Discussion

5.1 Analysis by Particle Size

Using the dry sieving method, not all particles could be completely separated, resulting in smaller particles sticking to larger ones. Nevertheless, this method was the most suitable choice compared to wet sieving, and led to effective separation with minimal effort. Introducing liquid into the gravel during wet sieving would have led to a loss of ^{137}Cs from the sample.

As expected, the measured activity concentrations correlate with particle size. The increasing surface area of smaller particles is the dominant factor for their higher activity concentrations. According to the general radiation protection ordinance of Austria [36], the limit for restricted clearance, i.e., the disposal of waste at a regular disposal site, for ^{137}Cs is $10\,Bq/g$. Material from the two largest fractions would therefore not need to be treated as radioactive waste on the site. For the actual waste sample EB9376, all measured activity concentrations for each fraction in this study were below the limits for restricted clearance. In this sample, this concerned the radionuclides ^{60}Co, ^{63}Ni, ^{90}Sr, ^{137}Cs, ^{241}Pu and ^{241}Am.

During the depth profile analysis, a notably high value was observed in the sample from the bottom. Fine fractions which tend to accumulate on the bottom of a container might have influenced the sample and have increased the ^{137}Cs activity concentration due to their larger surface area.

5.2 Dealing with Heterogeneous Samples

Large amounts of waste are not in a homogeneous state, which makes representative analysis challenging. Even contaminated gravel samples encounter the issue of inhomogeneities on a small scale, making it impossible to obtain truly identical subsamples. Depending on the required accuracy, homogenization before measurement can be applied. Grinding, already used when necessary, proved to be highly effective as shown in Figure 4.10. The representation of single samples for the whole material was improved by this method and results were significantly closer to the mean activity concentration with which the gravel was contaminated. While these time consuming preparation steps may not always be necessary, depending on the accepted errors and use, they enhance material homogeneity.

5.3 Examination of the Standard Routines for Digestion, Strontium Separation and LSC Spectra Evaluation

Both digestion methods did lead to sufficient dissolution of radionuclides for LSC, although some peculiarities were observed.Cesium is considered as a highly soluble element and complete digestion is expected. Observed was an incomplete digestion because only 72.7% (unfired sample) and 44% of the initial ^{137}Cs activity were recovered in the digestion solution.Similar behavior has been observed in other laboratory measurements. The residue that remains after filtering, the so called filter cake, contained twice as high (unfired sample) and almost the same (fired sample) ^{137}Cs activity concentration. For ^{241}Am, complete digestion was achieved with the unfired sample but, like with ^{137}Cs, a lower yield for the fired sample. ^{60}Co activity concentrations were lowest in the solid and results of following measurements were below the detection limit. Only in the residue of the fired sample a small yield was observed. A change in the filter cake composition was observed which has not yet appeared. Where the material originating from the unfired sample, digested using the beaker method, looked like powdered gravel after drying, the material from the fired sample and the microwave digestion appeared crumbly. Apparently the firing process and the digestion changed chemical bindings and produced hygroscopic particles potentially from $CaCO_3$ contents. Further investigation is needed to determine the exact cause.

In all previous measurements with gamma spectroscopy an apparent background from β-emitters within the spectra in the low energy range was seen. Based on experience in analysis of local radioactive waste, it was strongly suspected that a large share of activity in this waste originates from ^{90}Sr. However, the main goal and requirement for LSC in this study, quantifying ^{90}Sr activities in the gravel waste, was successfully achieved for all three techniques: Cerenkov counting, direct LSC and LSC of sample with strontium separation.

Due to the variety of nuclides seen in the LSC spectra, the regular deconvolution routine, described in chapter 3.8, was applied. Even though the process consists of manual spectrum fitting, the method provided good reproducibility and low deviations, shown in Table 4.1 and 4.2. The results also aligned with those from Cerenkov counting, which only depends on the detected counts in a certain energy range. This consistency validates the applied method, shows that no major errors are introduced and confirms its reliability. Due to firing the sample, ^{3}H could be extracted and a meaningful ^{241}Pu activity concentration was calculated. Through comparison of spectra by fired and unfired samples, an estimate for ^{3}H activity concentration could be given. Although there exist other methods to analyze Pu activity of a sample [37], the applied method might be useful if a full separation of all important nuclides or other techniques are too time-consuming. However, chemical separation like it was applied as ion exchange chromotography with strontium, may offer more exact results and should be applied when detailed characterization of single radionuclides is required.

Overall, results obtained by the different methods applied did not show great deviations for ^{90}Sr activity concentrations. However, it should be noted that both ^{90}Sr and ^{63}Ni have a lower activity concentration in the fired sample. Presumably firing in the furnace might volatilize a fraction of the nuclides.

5.4 XRF Method Review

The comparison of the three sample preparation methods for XRF in terms of their cost-benefit analysis provided useful insights for the routine work at NES. Preparation of samples with loose powder and pressed powder yielded similar results, making the loose powder method preferable due to its time efficiency. Furthermore it was observed that carbon correction failed for samples as pressed powder. Compared to the measured LOI, the calculated CO_2 ratios were overestimated in the pressed powder samples, likely due to the added wax.

5.5 Chemical Effects on Cesium Distribution

To investigate whether deviations in chemical composition could be correlated with ^{137}Cs activity concentrations, XRF analysis was conducted. Contrary to this assumption, no significant correlation was found. The surface effect, i.e., particle with greater surface area tend to keep more cesium on them, seems to be the dominant factor in the sample.

Samples taken from different depths of the original container showed only slight deviations in their elemental composition, without a trend. These differences were too small to establish any meaningful relationship with cesium activity or other interpretation.

In contrast, samples from the sieving analysis, both from upper and lower halves equally, consisted of deviating elemental compositions. Variations were observed for changes in SiO_2, MgO and CaO content. Thus quartz seems to be found more frequently in the medium-sized fractions, while the coarsest and finest particles more likely consist of minerals containg calcium and magnesium oxide, like limestone. The finest fraction showed an increasing Al_2O_3 content, which might origin in clay minerals that contain aluminum. The impact of these minerals and its possible influence on cesium abundance in finer fractions is worth further investigations. Quartz is a rather hard material and therefore less likely to be found in the smallest particles.

Chapter 6

Outlook

This study examined many of the sample preparation and detection methods currently in use at NES laboratories. These methods are sophisticated and well-established for their required applications. However, during the evaluation process, further questions emerged and require a closer look. Future demands, particularly those regarding the ongoing reconditioning processes, might require higher analytical capacity or adapted methods. A key observation for future applications in radioactive waste analysis is the increasing importance of grinding as a method for obtaining representative samples fast and effectively if needed.

The LSC spectra evaluation routine remains under continuous development due to newly evolving aspects of radioactive waste. For instance, contents of the radionuclide ^{63}Ni in the past were for a long time not quantified in LSC spectra due to its low activity ratio. However, EB9376 and other waste samples, which were analyzed during this study did show a noticeable ^{63}Ni signature in spectra. It might be suggested that ^{63}Ni has often been a more common component of the radionuclide inventory of samples than previously assumed.

Similarly, the separation of ^{3}H from assumed ^{241}Pu counts had not been subject of previous analysis, mainly because sample inventory has changed over recent years and a lack of necessity. Recording standard spectra for ^{241}Pu and ^{3}H with LSC could enable the same fitting, as applied for other radionuclides. Investigations on the separation of other elements apart from strontium could show the validation or deviations from results obtained by the current evaluation method. The LSC evaluation method is a manual process and requires time and experience to be performed correctly. Future work could focus on the automatization of the evaluation process and optimizing the standard spectrum fitting.

Furthermore, a second tin bucket containing gravel contaminated with ^{90}Sr was prepared simultaneously in spring 2023 with the waste investigated in this work and contains similar activity concentrations. It was not used for any applications either. This material could provide an opportunity for future investigations of ^{90}Sr distribution in gravel and a comparison with the findings of this study could be considered.

List of Figures

List of Tables

Bibliography

[1] *Eighth National Report of Austria*. Tech. rep. Federal Ministry Republic of Austria Climate Action, Environment, Energy, Mobility, Innovation and Technology – Department V/8 – Radiation Protection, 2024.

[2] W. Neckel, G Nittmann, and R Steininger. "Reconditioning of Historic Radioactive Waste in Austria: Experiences with and status of the project". In: *Radioactive Waste Management: Solutions for a Sustainable Future. Proceedings of an International Conference*. 2023.

[3] W. Neckel. *Rückbau der ehemaligen Schlammbeethalle*. Tech. rep. Nuclear Engineering Seibersdorf GmbH, 2010.

[4] H. Sicius. "Wasserstoff und Alkalimetalle: Elemente der ersten Hauptgruppe". In: *Handbuch der chemischen Elemente*. Springer, 2019, pp. 1–73.

[5] P. Melnikov and L. Z. Zanoni. "Cesium, Therapeutic Effects and Toxicity". In: *Encyclopedia of Metalloproteins*. Ed. by R. H. Kretsinger, V. N. Uversky, and E. A. Permyakov. New York, NY: Springer New York, 2013, pp. 590–594. isbn: 978-1-4614-1533-6. doi: 10.1007/978-1-4614-1533-6_352. url: https://doi.org/10.1007/978-1-4614-1533-6_352.

[6] J. A. Del Debbio. *Removal of cesium from a high-level calcined waste by high temperature volatilization*. Tech. rep. EG and G Idaho, Inc., Idaho Falls, ID (United States), Oct. 1994. doi: 10.2172/137291. url: https://www.osti.gov/biblio/137291.

[7] S. Yakunin. "Cesium in Gaseous Emissions from the Vitrification Technology of Radioactive Waste (Review of Scientific and Technical Information)". In: *Radiochemistry* 64.4 (2022), pp. 482–490. doi: https://doi.org/10.1134/S1066362222040026.

[8] *Decay data of ^{137}Cs*. http://www.lnhb.fr/Laraweb/. Accessed: 2025-06-06. 2025.

[9] R. Cornell. "Adsorption of cesium on minerals: a review". In: *Journal of radioanalytical and nuclear chemistry* 171 (1993), pp. 483–500. doi: https://doi.org/10.1007/BF02219872.

[10] G. Steinhauser et al. "Artificial radioactivity in environmental media (air, rainwater, soil, vegetation) in Austria after the Fukushima nuclear accident". In: *Environmental Science and Pollution Research* 20 (2013), pp. 2527–2534. doi: https://doi.org/10.1007/s11356-012-1140-5.

[11] M. A. Olatunji et al. "Influence of adsorption parameters on cesium uptake from aqueous solutions-a brief review". In: *RSC advances* 5.88 (2015), pp. 71658–71683. doi: 10.1039/c5ra10598f.

[12] J. Wang and S. Zhuang. “Removal of cesium ions from aqueous solutions using various separation technologies”. In: *Reviews in Environmental Science and Bio/Technology* 18 (2019), pp. 231–269. doi: https://doi.org/10.1007/s11157-019-09499-9.

[13] H. Rai and M. Kawabata. “The dynamics of radio-cesium in soils and mechanism of cesium uptake into higher plants: newly elucidated mechanism of cesium uptake into rice plants”. In: *Frontiers in plant science* 11 (2020), p. 528. doi: 10.3389/fpls.2020.00528.

[14] H. Qin et al. “Investigation of cesium adsorption on soil and sediment samples from Fukushima Prefecture by sequential extraction and EXAFS technique”. In: *Geochemical Journal* 46.4 (2012), pp. 297–302. doi: 10.2343/geochemj.2.0214.

[15] A. KITAMURA et al. “Analysis of Adsorption Behavior of Cesium onto Quartz Using Electrical Double Layer Model”. In: *Journal of Nuclear Science and Technology* 33.11 (1996), pp. 840–845. doi: 10.1080/18811248.1996.9732018. eprint: https://doi.org/10.1080/18811248.1996.9732018.

[16] S. Antkiw, H. Waesche, and F. Senftle. “Surface adsorption of Cs137 ions on quartz crystals”. In: *American Mineralogist* 41.3-4 (1956), pp. 363–366.

[17] B. Mercer, L. Ames, and P. Smith. “Cesium purification by zeolite ion exchange”. In: *Nuclear Applications and Technology* 8.1 (1970), pp. 62–69. doi: 10.13182/NT70-A28635.

[18] J. H. Sterba et al. “Adsorption characteristics of a clinoptilolite-rich zeolite compound for Sr and Cs”. In: *Journal of Radioanalytical and Nuclear Chemistry* 318 (2018), pp. 267–270. doi: 10.1007/s10967-018-6096-6.

[19] S. Kwon et al. “Relationship between zeolite structure and capture capability for radioactive cesium and strontium”. In: *Journal of Hazardous Materials* 408 (2021), p. 124419. issn: 0304-3894. doi: https://doi.org/10.1016/j.jhazmat.2020.124419. url: https://www.sciencedirect.com/science/article/pii/S0304389420324092.

[20] H. Y. Lee et al. “Selective removal of radioactive cesium from nuclear waste by zeolites: on the origin of cesium selectivity revealed by systematic crystallographic studies”. In: *The Journal of Physical Chemistry C* 121.19 (2017), pp. 10594–10608. doi: 10.1021/acs.jpcc.7b02432.

[21] E. Johan et al. “Natural zeolites as potential materials for decontamination of radioactive cesium”. In: *Procedia Environmental Sciences* 28 (2015), pp. 52–56. doi: https://doi.org/10.1016/j.proenv.2015.07.008.

[22] T. Abdollahi, J. Towfighi, and H. Rezaei-Vahidian. “Sorption of cesium and strontium ions by natural zeolite and management of produced secondary waste”. In: *Environmental Technology & Innovation* 17 (2020), p. 100592. doi: https://doi.org/10.1016/j.eti.2019.100592.

[23] H. Zhang et al. “Removal of Cesium from Radioactive Waste Liquids Using Geomaterials”. In: *Applied Sciences* 11.18 (2021). issn: 2076-3417. doi: 10.3390/app11188407. url: https://www.mdpi.com/2076-3417/11/18/8407.

[24] Y. Cho and S. Komarneni. “Cation exchange equilibria of cesium and strontium with K-depleted biotite and muscovite”. In: *Applied clay science* 44.1-2 (2009), pp. 15–20. doi: https://doi.org/10.1016/j.clay.2008.12.015.

[25] J. P. McKinley et al. “Microscale distribution of cesium sorbed to biotite and muscovite”. In: *Environmental Science & Technology* 38.4 (2004), pp. 1017–1023. doi: 10.1021/es034569m.

[26] G. Choppin et al. *Radiochemistry and nuclear chemistry*. Academic Press, 2013, pp. 262–274.

[27] G. F. Knoll. *Radiation detection and measurement*. John Wiley & Sons, 2000.

[28] R. Broda, P. Cassette, and K. Kossert. “Radionuclide metrology using liquid scintillation counting”. In: *Metrologia* 44.4 (2007), S36. doi: 10.1088/0026-1394/44/4/S06. url: https://dx.doi.org/10.1088/0026-1394/44/4/S06.

[29] *Decay data of ^{90}Sr and ^{90}Y*. http://www.lnhb.fr/Laraweb/. Accessed: 2025-05-05. 2025.

[30] P. Brouwer. “Theory of XRF”. In: *PANalytical BV* 59 (2010).

[31] G. Wurmbauer. “Messung von Retentionsprofilen von radioaktiv kontaminierter Erde und die Effizienz von Auslaugverfahren zur Minimierung des radioaktiven Abfalls”. Universität Wien, 2004, pp. 55–65.

[32] *Detector specification and performance data for BE2820*. Canberra. Technical data sheet. 2007.

[33] U. UNSCEAR et al. “Report to the General Assembly, with scientific annexes”. In: *United Nations* Volume 1 (2000), p. 116.

[34] *Product Sheet SR Resin*. Tech. rep. TRSIKEM International, 2015.

[35] H.-J. Weise and P. Fliss. *Identifikation von Beta-Nukliden und Analyse von Mehrfach-Beta-Spektren bei Messungen mit dem Flüssig-Szintillationsspektrometer (LSC)*. Tech. rep. Institut für Sicherheitsforschung und Reaktortechnik Jül-3066, 1995. url: http://hdl.handle.net/2128/21325.

[36] Republic of Austria. *Allgemeine Strahlenschutzverordnung 2020 (AllgStrSchV 2020)*. https://www.ris.bka.gv.at/Dokumente/BgblAuth/BGBLA_2020_II_339/BGBLA_2020_II_339.pdf. Bundesgesetzblatt II Nr. 339/2020, consolidated version. Accessed via RIS. 2020.

[37] T.-Y. Su and T.-L. Tsai. “Determination of plutonium-241 in low-level radwastes using radiochemical separation combined with LSC, alpha spectrometer and ICP-MS”. In: *Journal of Radioanalytical and Nuclear Chemistry* 319 (2019), pp. 447–452. doi: https://doi.org/10.1007/s10967-018-6362-7.

Appendix

Elemental Composition

	Loose	Err.	Loose*	Err.	Pressed	Err.	Pressed*	Err.	Disk	Err.
					C1					
Sum	71.9		100		69.3		100		100	
CO_2			31.4	0.7			34.8	0.1	20.5	
MgO	5.79	0.2	6.19	0.3	6.93	0.08	7.37	0.08	7.88	0.08
SiO_2	33.8	0.4	33.9	0.4	32.2	0.2	31.9	0.1	49.1	0.1
CaO	22.6	0.2	19.4	0.2	21.9	0.1	18.3	0.1	15.2	0.1
Al_2O_3	4.75	0.2	4.92	0.2	4.3	0.06	4.4	0.06	3.24	0.05
					C2					
Sum	74.3		100		68.2		100		100	
CO_2			30.1	0.6			36.6	0.1	20.8	
MgO	7.43	0.3	7.8	0.3	6.67	0.08	7.06	0.08	7.58	0.08
SiO_2	33.3	0.4	32.7	0.4	29.6	0.2	29.1	0.1	47.9	0.1
CaO	23.5	0.2	20	0.2	22.6	0.1	18.7	0.1	15.9	0.1
Al_2O_3	5.21	0.2	5.28	0.2	4.6	0.06	4.69	0.06	3.54	0.06
					C3					
Sum	71.4		100		67.1		100		100	
CO_2			30.7	0.6			36.2	0.1	20.2	
MgO	7.04	0.3	7.64	0.3	7.23	0.08	7.78	0.08	7.47	0.08
SiO_2	34.7	0.4	35.1	0.4	32.2	0.2	32.2	0.1	49.4	0.1
CaO	20.4	0.2	17.8	0.2	19.8	0.1	16.6	0.1	15.4	0.1
Al_2O_3	4.73	0.2	4.94	0.2	3.71	0.06	3.83	0.06	3.56	0.06
					C4					
Sum	73.4		100		65.6		100		100	
CO_2			27.3	0.6			36.5	0.1	19.3	
MgO	6.82	0.3	7.44	0.3	6.84	0.08	7.52	0.08	6.96	0.08
SiO_2	36.6	0.4	37.6	0.4	31.2	0.2	31.9	0.1	51	0.1
CaO	20.8	0.2	18.7	0.2	19.5	0.1	16.7	0.1	14.9	0.1
Al_2O_3	4.63	0.2	4.89	0.2	3.85	0.06	4.06	0.06	3.72	0.06
					C5					
Sum	73.3		100		64		100		100	
CO_2			28.5	0.6			38.6	0.1	20.4	
MgO	7.74	0.3	8.36	0.3	7.11	0.08	7.82	0.08	7.62	0.08
SiO_2	34.1	0.4	34.6	0.4	27.8	0.2	28.4	0.1	48.9	0.1

CaO	22.4	0.2	19.9	0.2	21.5	0.1	18.2	0.1	15.4	0.1
Al_2O_3	4.53	0.2	4.72	0.2	3.73	0.06	3.93	0.06	3.51	0.06
					C6					
Sum	76.6		100		72.5		100		100	
CO_2			19.8	0.4			29	0.1	18.1	
MgO	6.48	0.3	7.26	0.3	6.52	0.08	7.03	0.08	6.98	0.08
SiO_2	42.6	0.5	45.7	0.5	39.3	0.2	39.9	0.1	54.1	0.1
CaO	18.2	0.2	17.8	0.2	18.4	0.1	16.2	0.1	13.3	0.1
Al_2O_3	4.34	0.2	4.75	0.2	4.08	0.06	4.26	0.06	3.24	0.05
					C7					
Sum	74.5		100		73.4		100		100	
CO_2			23.3	0.5			26.9	0.1	19	
MgO	4.78	0.2	5.33	0.2	5.78	0.07	6.28	0.07	6.43	0.07
SiO_2	43.3	0.5	46	0.5	41.8	0.2	43.1	0.1	50.3	0.1
CaO	17.8	0.2	16.8	0.2	17.8	0.1	16	0.1	15.3	0.1
Al_2O_3	3.65	0.2	3.97	0.2	3.73	0.06	3.94	0.06	3.98	0.06
					C8					
Sum	76.6		100		72.4		100		100	
CO_2			20.6	0.4			26.5	0.1	17.7	
MgO	6.09	0.2	6.76	0.3	5.85	0.07	6.45	0.07	6.19	0.07
SiO_2	45.6	0.5	48.3	0.5	43	0.2	45	0.1	54.5	0.1
CaO	16.8	0.2	16.1	0.2	16.6	0.1	15.2	0.1	13.9	0.1
Al_2O_3	3.64	0.2	3.94	0.2	3.23	0.05	3.46	0.05	3.34	0.05
					C9					
Sum	73.3		100		71.6		100		100	
CO_2			24.5	0.5			28.2	0.1	20	
MgO	7.21	0.3	8.07	0.3	7.21	0.08	7.91	0.08	7.68	0.08
SiO_2	40.8	0.5	43.2	0.5	39.9	0.2	41.3	0.1	49.7	0.1
CaO	17.5	0.2	16.4	0.2	17.5	0.1	15.8	0.1	14.8	0.1
Al_2O_3	3.4	0.1	3.69	0.2	3.18	0.05	3.38	0.05	3.35	0.05
					C10					
Sum	74		100		72.8		100		100	
CO_2			25.7	0.6			28.5	0.1	17.5	
MgO	4.31	0.2	4.74	0.2	5.72	0.07	6.16	0.07	6.11	0.07
SiO_2	40.8	0.5	42.4	0.5	39.5	0.2	40.2	0.1	54	0.1
CaO	18.9	0.2	17.4	0.2	18.6	0.1	16.5	0.1	13.8	0.1
Al_2O_3	4.82	0.2	5.16	0.2	4.64	0.06	4.85	0.06	3.87	0.06

					Simulate					
Sum	71.9		100		73.6		100		100	
CO_2			25.7	0.6			32.4	0.1	27.5	
MgO					0.352	0.02	0.365	0.02	0.322	0.02
SiO_2	31.9	0.4	35.5	0.4	30.6	0.2	30.9	0.1	32.4	0.1
CaO	38.9	0.3	37.7	0.3	42.2	0.2	35.8	0.1	35.1	0.1
Al_2O_3	0.098	0.02	0.111	0.03	0.122	0.01	0.125	0.01	0.108	0.01
					Original gravel					
Sum	71.6		100		67.7		100		100	
CO_2			29.6	0.6			36.5	0.1	27.4	
MgO	9.99	0.3	11	0.4	9.64	0.09	10.3	0.09	10.8	0.09
SiO_2	29.6	0.4	30.4	0.4	26.7	0.2	26.6	0.1	37.7	0.1
CaO	26.2	0.2	23.4	0.2	26.4	0.2	22.2	0.1	19.9	0.1
Al_2O_3	2.64	0.1	2.77	0.1	2.33	0.05	2.37	0.05	1.96	0.04
					SiO_2					
Sum	73.8		100		83.8		100		100	
SiO_2	73.2	0.6	99.2	0.8	83.1	0.3	99.1	0.08	89.4	0.2
					CaCO3					
Sum	70.3		100		70.8		100			
CO_2			41.1	1			43.9	0.2		
CaO	69	0.4	57.6	0.3	69.8	0.3	55.2	0.1		

Table A.1: The results obtained by XRF analysis of samples of the depth profile and comparison samples. The elemental compositions of the most abundant components obtained by the three different preparation methods, which were investigated, are summarized and sorted by sample. All values are given as a percentage. C1 represents the layer closest to the surface of the container, while C10 represents the bottom layer. For loose powder and pressed powder samples, the CO_2 content was added by the software via detected Compton scattering and is shown as Loose* and Pressed*. The values are normalized to 100 %. The CO_2 content of the solid disks was computed based on the assumption that *MgO* and *CaO* were present as carbonate before ignition and added after evaluation. For the simulate a water content of 3.59 % was calculated. For SiO_2 a LOI of 9.98 % was measured, which sums up with the measured SiO_2 content to approximately 100 %. Rows, which depict the sum, indicate the ratio of components actually detected or calculated by the XRF software in the sample. The sum does not match the sum of the oxides, because only the most abundant oxides are included.

	EB9376					
	Loose*	Err.	Pressed*	Err.	Disk	Err.
CO_2	37.3	0.9	44.4	0.2	32.3	
MgO	6.01	0.3	5.84	0.07	8.51	0.08
SiO_2	16.9	0.3	13.4	0.1	24	0.1
CaO	32.2	0.2	30.2	0.1	29.3	0.1
Al_2O_3	2.93	0.1	2.24	0.04	2.16	4
Fe_2O_3	2	0.06	1.9	0.04	1.53	0.04
P_2O_5	1.49	0.04	0.793	0.03	0.433	0.02

Table A.2: Elemental composition of real waste sample EB9376. Analogous to samples in table A.1 all three preparation methods were applied. Loose* and Pressed* indicate, that CO_2 content was added according to the software evaluations.

	DO1		DO0.5		DO0.25		DO0.125		DO0.063		DOB	
	Conc.	Err.	Conc.	Err.	Conc.	Err.	Conc.	Err.	Conc.	Err.	Conc.	Err.
CO_2	26.5		20.3		10.9		11.8		16.5		23	
MgO	10.4	0.09	7.27	0.08	3.53	0.06	3.51	0.06	4.87	0.06	7.43	0.08
SiO_2	39.9	0.1	49.8	0.1	68.9	0.1	63.3	0.1	44.5	0.1	31.6	0.1
CaO	19.3	0.1	15.8	0.1	8.99	0.09	10.1	0.09	14.2	0.1	19	0.1
Al_2O_3	1.87	0.04	2.96	0.05	3.36	0.05	5.46	0.07	7.07	0.08	8.64	0.08
Fe_2O_3	0.97	0.03	1.15	0.03	1.22	0.03	2.03	0.04	2.83	0.05	3.53	0.06
	DU1		DU0.5		DU0.25		DU0.125		DU0.063		DUB	
	Conc.	Err.	Conc.	Err.	Conc.	Err.	Conc.	Err.	Conc.	Err.	Conc.	Err.
CO_2	26.6		19.6		10.6		11.4		17.3		22.8	
MgO	10.7	0.09	7.04	0.08	3.47	0.05	3.39	0.05	5.17	0.07	7.36	0.08
SiO_2	39	0.1	51.5	0.1	69.6	0.1	64.1	0.1	46.5	0.1	31.9	0.1
CaO	19	0.1	15.2	0.1	8.69	0.08	9.76	0.09	14.9	0.1	18.8	0.1
Al_2O_3	1.95	0.04	2.93	0.05	3.36	0.05	5.32	0.07	7.43	0.08	8.71	0.08
Fe_2O_3	1	0.03	1.09	0.03	1.18	0.03	2.01	0.04	3.06	0.05	3.47	0.05

Table A.3: Elemental composition of samples of the grain size analysis. For these samples only glass disks were prepared and measured. All values are given in percent and concentrations for CO_2 were calculated with *CaO* and *MgO* content.

Loss on Ignition

	LOI	Calculated	LOI/Calc.
C1	21.457	20.533	1.045
C2	21.792	20.755	1.050
C3	21.159	20.243	1.045
C4	20.251	19.293	1.050
C5	21.416	20.406	1.049
C6	18.809	18.059	1.042
C7	20.305	19.029	1.067
C8	18.832	17.668	1.066
C9	20.934	20.001	1.047
C10	18.474	17.502	1.056
DO1	26.476	26.503	0.999
DO0.5	21.290	20.338	1.047
DO0.25	11.961	10.910	1.096
DO0.125	12.961	11.759	1.102
DO0.063	23.361	16.462	1.419
DOB	26.490	23.024	1.151
DU1	26.970	26.595	1.014
DU0.5	20.486	19.616	1.044
DU0.25	11.602	10.609	1.094
DU0.125	12.732	11.361	1.121
DU0.063	19.544	17.339	1.127
DUB	26.383	22.791	1.158
EB9376	32.770	32.287	1.015

Table A.4: Loss on ignition and calculated loss of CO_2 of each sample. LOI was computed by the weight differences of the crucibles before and after firing the samples. The CO_2 content was calculated with the *MgO* and *CaO* contents obtained by XRF as in Tables A.1, A.3 and A.2.

Übersicht verwendeter Hilfsmittel

Zur Unterstützung bei der sprachlichen Formulierung einzelner Passagen wurde für wenige Sätze ein Übersetzungstool (DeepL Translator) eingesetzt.